2012

Analytical Chemical Sensing Using High Resolution Terahertz/ Submillimeter Wave Spectroscopy

Benjamin L. Moran
Wright State University

ANALYTICAL CHEMICAL SENSING USING HIGH RESOLUTION TERAHERTZ/SUBMILLIMETER WAVE SPECTROSCOPY

A thesis submitted in partial fulfillment of the requirements for the degree of Master of Science

By

Benjamin Lee Moran
B.S. in Applied Physics, Thiel College, 2010

2012
Wright State University

WRIGHT STATE UNIVERSITY

GRADUATE SCHOOL

August 24, 2012

I HEREBY RECOMMEND THAT THE THESIS PREPARED UNDER MY SUPERVISION BY Benjamin L Moran ENTITLED Analytical Chemical Sensing Using High Resolution Terahertz/Submillimeter Wave Spectroscopy BE ACCEPTED IN PARTIAL FULFILLMENT OF THE REQUIREMENTS FOR THE DEGREE OF Master of Science.

_____
Ivan R. Mevedev, Ph. D.
Thesis Director

_____
Doug Petkie Ph. D.
Chair, Department of Physics

Committee on
Final Examination

_____
Ivan Medvedev Ph.D.

_____
Doug Petkie Ph.D.

_____
Gary Farlow Ph.D.

_____
Andrew Hsu Ph. D.
Dean, Graduate School

ABSTRACT

Moran, Benjamin Lee. M.S. Department of Physics, Wright State University, 2012. Analytical Chemical Sensing Using High Resolution Terahertz/Submillimeter Wave Spectroscopy

A highly sensitive and selective Terahertz gas sensor used to analyze a complex mixture of Volatile Organic Compounds (VOCs) has been developed. To best demonstrate analytical capabilities of a THz chemical sensor, we chose to perform analytical quantitative analysis of a certified gas mixture using a prototype gas phase chemical sensor that couples a commercial preconcentration system (Entech 7100A) to a custom high resolution THz spectrometer. A Method TO-14A certified mixture of thirty-nine VOCs was purchased. Twenty-six of the thirty-nine chemicals were identified as suitable for THz spectroscopic detection. The Entech 7100A system is designed and marketed as an inlet system for Gas Chromatography Mass Spectrometry (GC-MS) instruments with a specific focus on TO-14A sampling methods and has been incorporated into our spectrometer. Its preconcentration efficiency is high for the thirty-nine chemicals in the mixture used for this study and our preliminary results confirm this for many of the selected VOCs. Presented are the results of this study which will serve as a basis for our ongoing research in environmental sensing and exhaled human breath.

Table of Contents

List of Figures

List of Tables

Chapter 1

1.1 Introduction

There are a wide variety of chemical sensors and applications of those sensors. Applications of various chemical sensors include clinical, industrial, environmental, agricultural, and military technologies and can range in importance from medical diagnosis to national security [1] [2]. This thesis will focus on the development of a new gas phase analytical chemical sensor capable of analyzing complex atmospheric chemical mixtures with the long-term goal of being able to examine human breath and environmental mixtures. The gas phase analytical chemical sensor consists of a custom THz spectrometer coupled to a chemical preconcentrator. This setup will be discussed later in Chapter 2. Along with results of this experiment, the preliminary results and a discussion of breath analysis can also be seen in Chapter 3.

1.2 Terahertz/Submillimeter

The THz frequency range, as it is currently defined, is from 100 GHz (λ = 3mm) to 10 THz (λ = 0.03mm). The THz range is described by many scientists as the most scientifically useful frequency range, because of the quantity of molecular species that are active in the region and the properties of THz waves. THz is used by a wide variety of scientists including chemists, astronomers, and atmospheric scientists. Chemists use THz to study the structure and the dynamics of molecules [3]. Astronomers use the technology to identify molecules in space to better understand the universe [4]. Atmospheric Scientists use THz to trace different constituents that are present in the atmosphere [5]. Our goal is to be able to detect human breath.

The THz frequency range, although scientifically important, has been one area of the spectrum that has been difficult to investigate. The main difficulty was not having affordable technology that had the ability to function throughout the THz spectral range. With advancements in technology driven by ultrafast time domain spectroscopists and radio astronomers, THz sources are readily available in a variety of technologies [6]. THz radiation sources available today can either be a fundamental source or a synthesized source. Fundamental sources are sources that are either free electron based or laser based. Free electron sources consist of Backward Wave Oscillator (BWO), Traveling Wave Tubes (TWT), Klystrons, and Gyrotrons [7]. Laser based fundamental sources are Quantum Cascade lasers (QCL) [7]. Synthesized sources also consist of two different types; electronic solid-state sources and optical sources. The most common type of solid state sources are diode multipliers such as Virginia Diode's (VDI) diode multiplier systems [8]. Optical sources are either pulsed or continuous wave, and are laser-driven [7].

All the different types of THz sources have their limitations and complexities. The source that was used for this thesis was a VDI diode multiplier system (Figure 1). The VDI system used is a multiplier system that uses a heterodyne receiver and functions in the 210-270 GHz range. The VDI system was selected because it was readily available, has high spectral resolution, and the capability to work effectively with lower power levels. These advantages are all described in more detail later in this chapter in Section 1.5 Advantages of Rotational Spectroscopy.

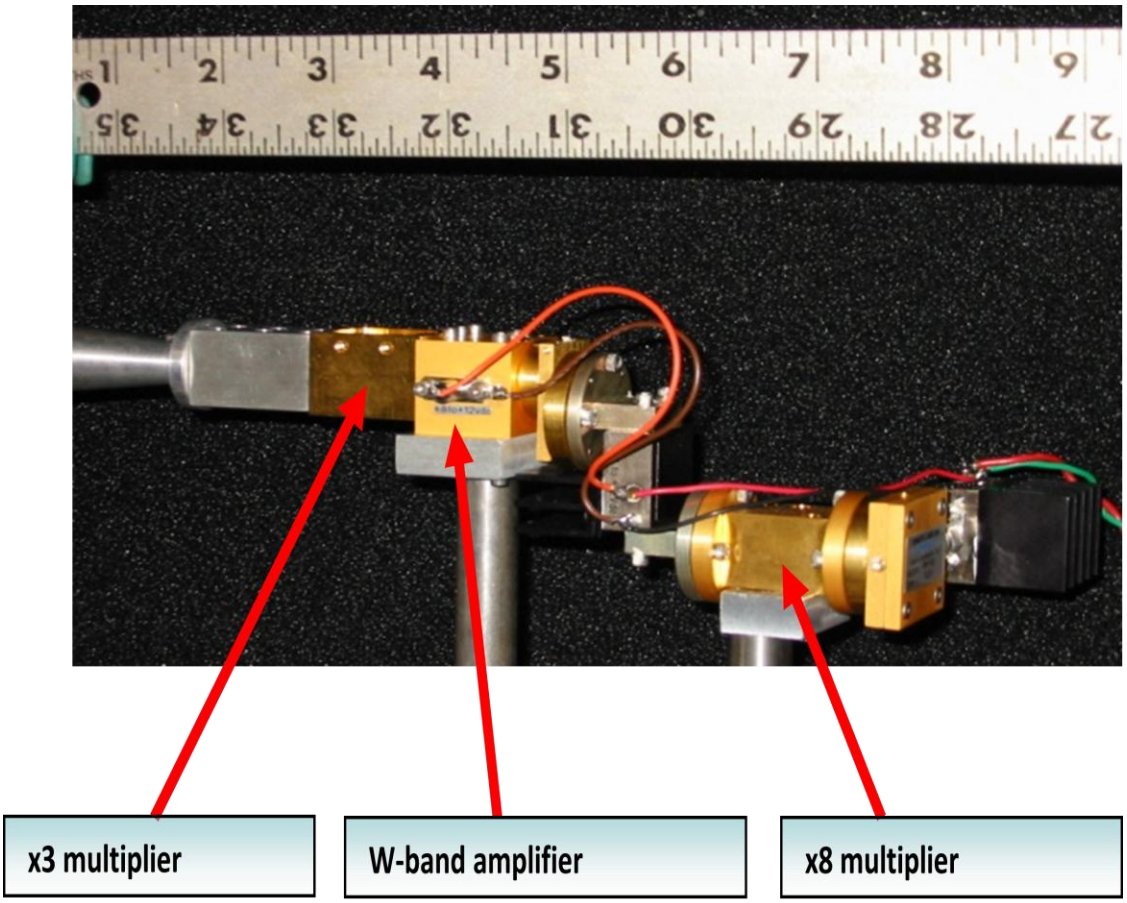

Figure 1 : Example of a VDI Multiplier Chain (Scale is in inches)

1.3 Rotational Spectroscopy

The THz range is the area of the electromagnetic spectrum in which molecular rotational energy transitions occur (Figure 2). Rotational spectra only exist in polar molecules. Polar molecules are molecules which have a permanent nonzero electric dipole moment or magnetic dipole moment. Electric dipole allowed transitions are generally stronger than magnetic transitions. Homonuclear diatomic molecules such as O_2 do not posses permanent electric dipole moments but due exhibit a permanent magnetic dipole moment. The simplest case of rotational spectroscopy to consider is from a rigid, linear diatomic molecule (Figure 3).

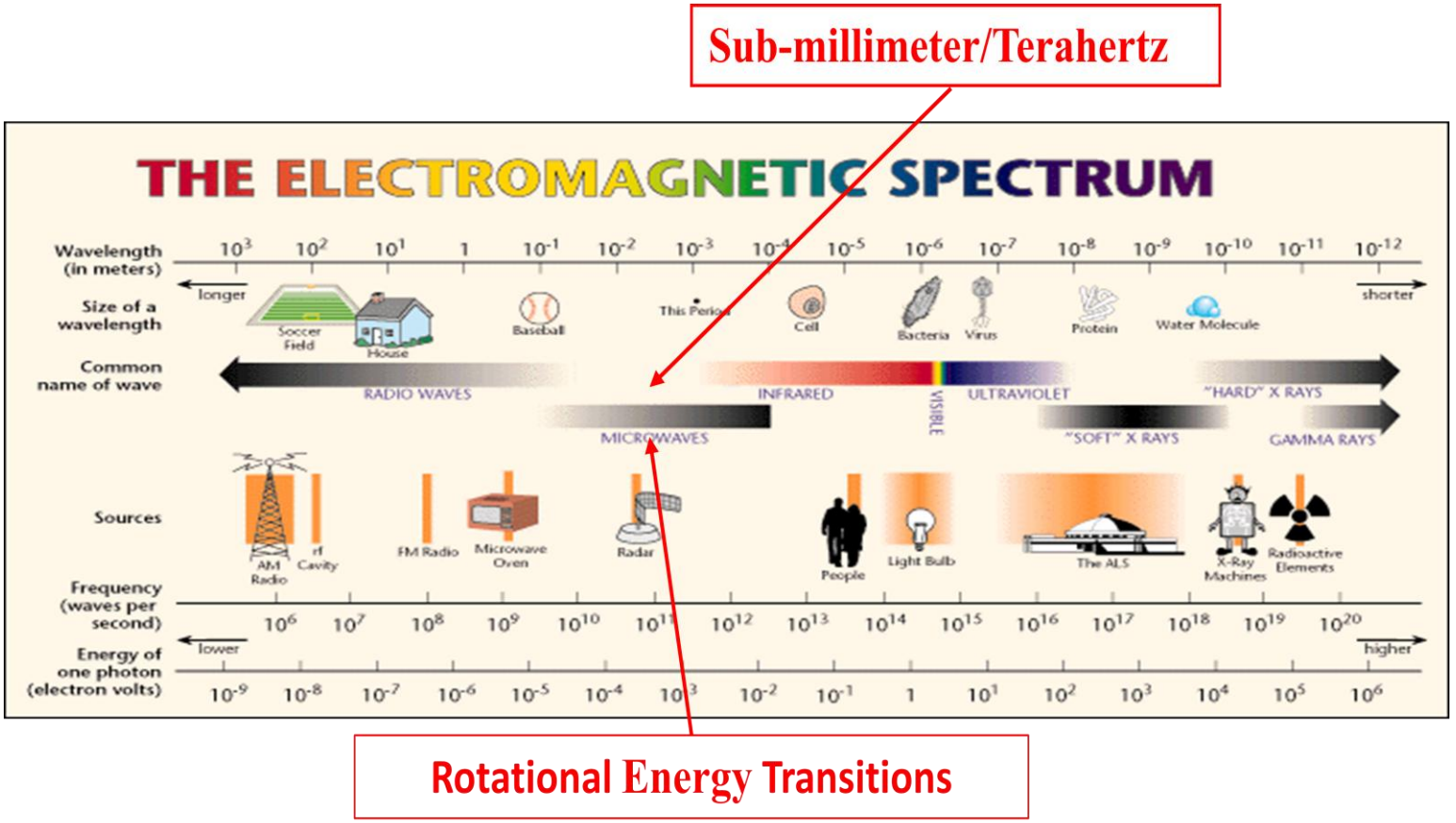

Figure 2 : Electromagnetic Spectrum

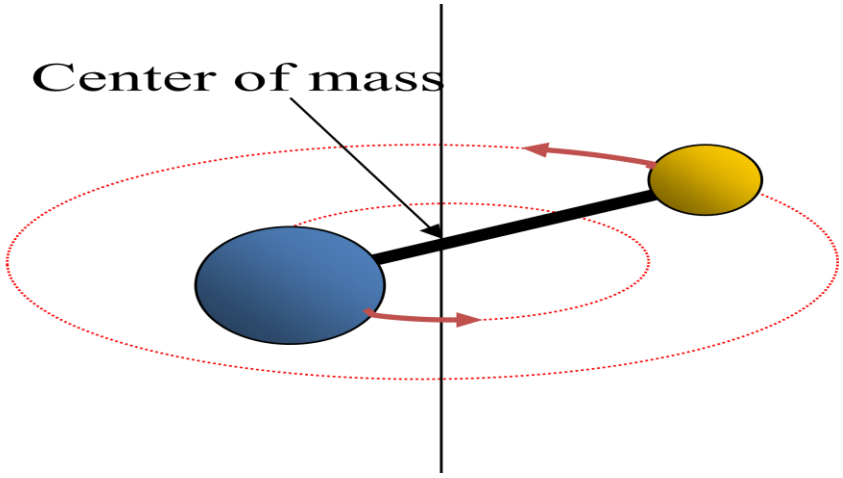

Figure 3 : Example of a Diatomic Molecule

Classically in the case of a rigid linear molecule in the principle axis frame, which has no net orbital, or spin angular momentum, and no linear momentum, the kinetic energy can then be described as Equation 1 [11].

$$\boldsymbol{E_{KE} = T = \frac{1}{2} I_x \omega_x^2 + \frac{1}{2} I_y \omega_y^2 + \frac{1}{2} I_z \omega_z^2} \qquad \text{Equation 1}$$

For a linear molecule, $I_z=0$ and using **P** to represent the total angular momentum.

$$T = \frac{1}{2} I_x \omega_x^2 + \frac{1}{2} I_y \omega_y^2 = \frac{\boldsymbol{P}_x^2}{2I_x} + \frac{\boldsymbol{P}_y^2}{2I_y} = \frac{\boldsymbol{P}^2}{2I}$$
$$I = I_x = I_y\,, \quad I_z = 0$$

Next, considering the case of a rigid rotor in isotropic space, the Hamiltonian can be expressed as Equation 2.

$$\boldsymbol{H = \frac{P^2}{2I}} \qquad \text{Equation 2}$$

Then, using the Hamiltonian, the energy can be found using Schrodinger's Equation 2.

$$\boldsymbol{\frac{P^2}{2I}\ \psi = E\psi}$$

$$\frac{\boldsymbol{P}^{\boldsymbol{2}}}{\boldsymbol{2I}}\boldsymbol{\psi} = \frac{\boldsymbol{J(J+1)}\hbar^{\boldsymbol{2}}\boldsymbol{\psi}}{\boldsymbol{2I}} = \boldsymbol{BJ(J+1)\psi} \qquad \boldsymbol{B} = \frac{\hbar^{\boldsymbol{2}}}{\boldsymbol{2I}} \qquad \text{Equation 3}$$

The rotational constant (*B*) is dependent on the specific geometry of each molecule and is inversely proportional to the moment of inertia. An interesting feature that arises from the *B* rotational constant is that every *2B* there is a periodicity within the spectra. This feature comes from the derivation of the energy shift between two adjacent *J* states. As can be seen from Equation 4, the frequency shift is *2B (J+1).* Electric dipole allowed transitions obey selection rules of $\Delta J = \pm 1$. Therefore, within each chemical spectrum one will find that every *2B* there will be significant clusters of spectral lines. For example, Chloroform has a *B* constant of 3.28 GHz, so roughly every 6.56 GHz there will be clusters of spectral lines as seen in Figure 4.

Figure 4 also allows us to view the excited vibrational states which can also be detectable in rotational spectra. The excited vibrational states, although weaker than ground state, do have spectra that are strong enough for detection, which can cause some potential issues. The main issue is that spectral lines from the vibrational states can cause spectral clutter. Clutter will be discussed in more detail in Chapter 3.

$$\boldsymbol{E_J = BJ(J+1)}$$

$$\boldsymbol{f_{(J+1)\rightarrow J} = B(J+1)(J+2) - BJ(J+1) = 2B(J+1)} \qquad \text{Equation 4}$$

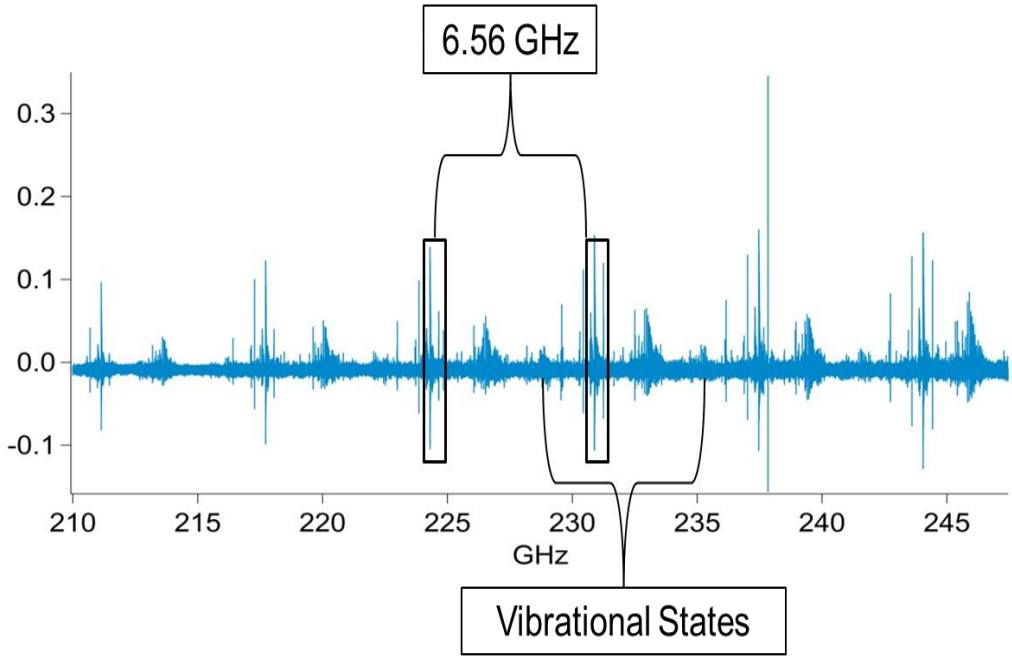

Figure 4 : Chloroform Spectrum with clumps of spectral lines every *2B* or 6.5 GHz

The different rotational constants also play a valuable role in the overall intensity and ability to detect various chemicals. An important graph that provides insights into effects of different *B* constants can be seen in Figure 5. In Figure 5, the distribution of the states is Boltzmann or Gaussian, which indicated thermal or excitation distributions. Now, following Figure 5, 25 GHz corresponds to a "light" molecule whereas 0.1 GHz corresponds to a "heavy" molecule. As molecular moments of inertia increase, their rotational constants decrease. As the rotational constants decrease, the density of lines within a spectrum increases and the spectral intensity decreases. Many of the molecules that are examined in this thesis have larger rotational constants; therefore the majority of the chemicals that were selected are in the range of the middle three graphs (Figure 5). This is ideal for our sensor because it operates in the 210-270 GHz range. Also, as the rotational constants decrease, the maximum intensity of the peaks shifts to the lower frequency. This allows for spectral lines near maximum to be examined since the sensor operates

in the 210 to 270 GHz range. Having the capability to view spectral lines of molecules near maximum intensity allows for detection with maximum sensitivity.

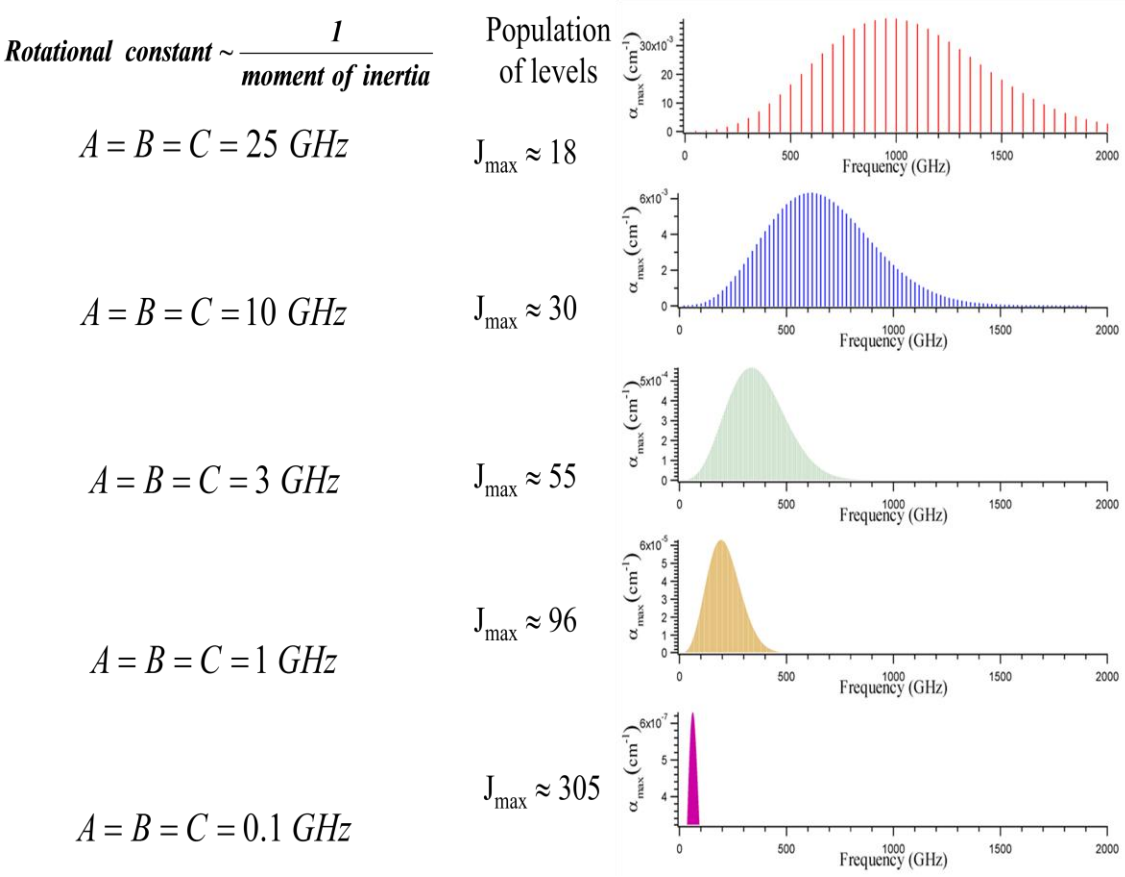

Figure 5 : Spectra as a Function of Molecular Size

1.4 Pressure Broadening

If the pressure within the sample becomes excessive pressure broadening may occur. Pressure broadening affects the overall spectral profile, which has a contribution from the overall pressure of the sample. Pressure broadening arises from the collisional interaction of the molecules [11]. Pressure broadening can happen with the identical molecules interacting with each other or interactions that may occur within a mixture. Experimentally, it has been found that typical pressure broadening coefficients are about 10 MHz/Torr [11]. This effect can have a substantial effect on the data. For instance, our sensor generally operates at 1 mTorr, therefore if a gas experiences pressure broadening our sensor will detect a line that pressure broadens at 10

kHz. The typical linewidth of the spectra seen throughout this thesis, which is only Doppler limited, is about 1 MHz. Therefore, if the sensor is operating at 1 mTorr then there will be about a 10 kHz broadening to the spectral line.

Limiting the pressure broadening is important because colliding molecules can have variable intensity and lineshapes based on the pressure. Therefore, pure sample library spectra and mixtures can vary from pressure to pressure, based on the molecular collisions which are more frequent at higher pressures. In pure samples, as the pressure increases, the sample pressure reaches a point where the intensity stops to increase as the lineshape broadens. This also happens in mixtures, but is less common with our sensor because the preconcentrator eliminates air constituents that would cause pressure broadening within a mixture. Limiting the sample pressure, allows the spectra to only be Doppler broadened [10]. Doppler broadening is a contribution to the overall linewidth which comes from the thermal motion of the molecules traveling towards and away from the detector. For rotational spectroscopy in the THz spectral range, Doppler broadening typically sets the limit on the resolution of spectra [10].

1.5 Advantages of Rotational Spectroscopy

There are several scientific advantages of using rotational spectroscopy for chemical detection. The first advantage is that spectral signatures are extremely sensitive to conformational and isotopic changes of molecular structure. The *B* rotational constants are rapidly changing due to changes in the molecular structure. Because of the changes in structure, it is essential to have a chemical sensor that has a high accuracy of the measured frequencies of molecular transitions. The frequency accuracy comes from the accuracy of our input clock which outputs a very accurate 10 MHz ($\pm 5 \times 10^{-11}$ MHz). Along with the high accuracy of the input source, the sensor also has high resolution. The sensor is capable of resolving lines with a linewidth of ~1 MHz only limited by the Doppler linewidth. The sensor being Doppler limited, allows for a high number of resolution elements (~100000). Other chemical sensors, such as Gas

Chromatography-Mass Spectrometry (GC-MS), have a much lower number of resolution elements (~200). The higher resolution allows for a chemical sensor with a much higher specificity.

Additionally, the energy level separations between states are much less than *kT*, which results in a large number of thermally populated energy levels. To get a better understanding, refer back to Figure 5 and the rotational constants of the selected chemicals from Table 2, which can be seen in Chapter 2. The majority of the chemicals that were focused on in this thesis are in the middle three graphs of Figure 5. The chemicals in the middle three graphs have small energy level separations and thus a large quantity of populated energy levels.

Another advantage is that the total amount of sample needed for analysis is small and static. The absolute sample size can approach a few femtogram(10^{-15}g) for an analyte which experiences near one-hundred percent absorption at full power (Appendix B). This absolute sample size is similar in comparison with other spectroscopic sensors operating in other spectral ranges. For example, GC-MS sensors can have absolute sample sizes that can be detected in low femtogram amounts (10^{-15}g) [12] [13] [14]. A major advantage of our sensor is that is uses an intensity calibration, which is reliant on spectral libraries, instead of a calibration standard. GC-MS requires the use of a calibration standard before a mixture can be analyzed.

The sensor is also highly sensitive and thus can approach the fundamental noise limits set by the mixing of the radiation generated by the source and the thermal background fluctuations. These noise limits are also referred to as Townes noise [15]. To calculate the Townes noise, Equation 5 is used where P_d is power of the detector (15 μW calculated in Section 2.1 Experimental Procedure), κ is Boltzmann constant, T=1000 K (noise temperature of the detector), and $\Delta v = 1/\Delta t$ where Δt is the time spent per point [16]. This results in a full power to noise of nearly 1.7 x 10^6. The chemical mixture, which is used in this thesis is a 1 ppm (one part per

million) dilution. For the stronger analytes (signal to noise ratio close to 2000) the sensor has the capability to approach detection at 500 ppt (part per trillion). Experimentally, the sensor has detected the analytes with stronger spectra with a full power to noise ratio of 10^5, which is one order of magnitude from the theoretical limit.

$$\frac{S}{N} = \sqrt{\frac{P_S}{\kappa T \Delta v}} \qquad \text{Equation 5}$$

$$\frac{S}{N} = \sqrt{\frac{15\ \mu W}{\left(1.38x10^{-23}\frac{m^2}{kgs^{-2}}\right)(1000K)\left(\frac{1}{0.018s}\right)}} \approx 4x10^6$$

1.6 First Spectrometer

The first commercially available microwave spectrometry system was introduced by Hewlett Packard (HP) in 1971 and was based on the technology that was developed in 1947 [17]. The HP 8460 was a molecular rotational resonance spectrometer capable of recording spectra from a range of 8 - 40 GHz [18]. The HP spectrometer was bulky and it cost $50,000 in 1971 (with inflation it would cost roughly $300,000 today). Only being able to reach 40 GHz limited the wide range functionality. It also required approximately one-hundred hours to complete a full scan at full sensitivity. The duration of our scans was typically 10 minutes. The overall length of the scan depends on various settings and the desired range. Because of the limitations of the HP8460 and the fact that spectroscopic computing was also limited at the time, the device was mainly used by structural chemists [18] [10]. However, it did provide the potential for the field of molecular rotational spectroscopy which has greatly advanced since 1971.

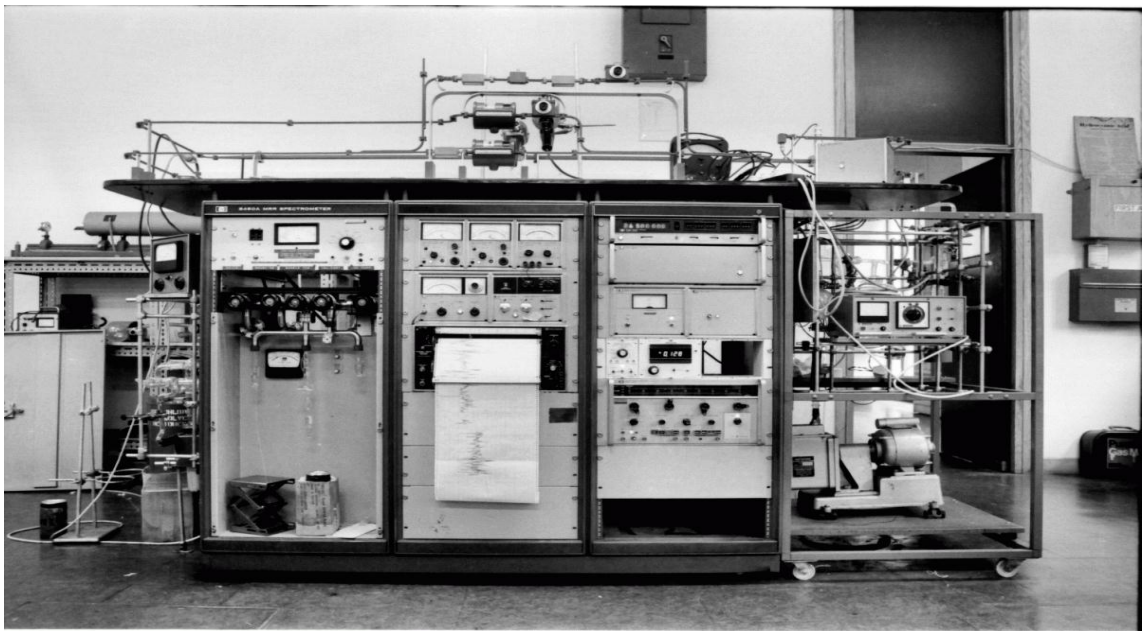

Figure 6 : The HP 8460 MRR (Molecular Rotational Resonance) introduced in 1971 [18].

1.7 Prior Work

Most recently, The Ohio State University (OSU) developed a chemical sensor similar to the one that will be discussed in this thesis [10]. OSU built a chemical sensor, which was self-contained in a one cubic foot box (Figure 7). Their sensor included gas handling and computation from within the box. Technologically both OSU's experiment and the one described throughout this thesis used very similar equipment. For more detail about the types of technology used in both experiments see Chapter 2. In the time frame they had, they were able to record a spectrum of thirty gases, but from a mixture of pure gas samples (without preconcentration). They were able to do preconcentration of one analyte. With the preconcentration of the one analyte, their sensor returned a sensitivity of approximately 2 ppt [10]. Their sensor has the capability to analyze either a prepared mixture or a dilute sample of air. One thing that they were unable to address was how a complex mixture would react with different sorbents in the preconcentrator. Having an understanding of the reaction of different sorbents with the mixture

can be a vital part in chemical sensor design. The importance of sorbents and other preconcentration features will be discussed in detail in Chapter 2.8 Preconcentration.

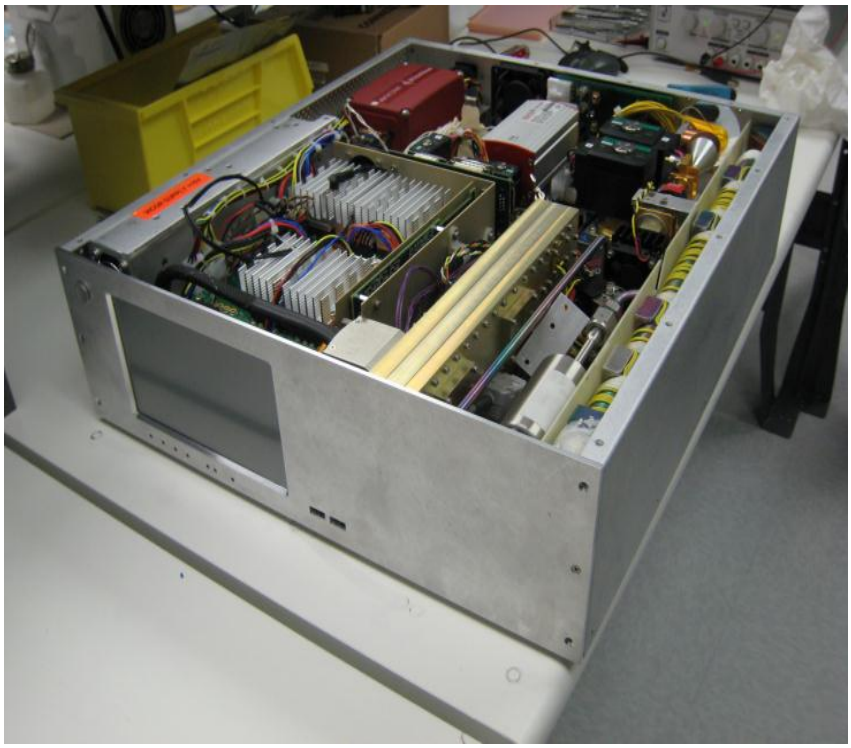

Figure 7 : Chemical Sensor made at OSU.

Chapter 2

2.1 Experimental Procedure

The thesis was based on a room temperature harmonic multiply chain as a source and a heterodyne receiver made by Virginia Diodes (VDI) [8]. The VDI system was used in conjunction with a custom built microwave synthesizer that drives the multiplier chain. The VDI system that was used has the capability of generating and detecting radiation in the 210 to 270 GHz range. This range was selected for several reasons. One reason is the region is less spectrally congested than other regions of the spectrum. The lack of spectral congestion allows the sensor to have the ability to look at molecules that are more difficult to detect in other regions of the spectrum. Another reason is that there are only a few air constituents that are spectrally active in the region (oxygen, nitrogen, argon, and carbon dioxide).

A heterodyne receiver was selected because it is capable of achieving better S/N at lower power levels. Lower power levels are necessary to prevent molecular power saturation. Sensitivity can become an issue with regular diode detectors especially when attempting to detect weaker analytes. Using a heterodyne receiver allows us to detect weaker species than when a regular diode detector is used. This happens because with the regular diode detector, spectral lines of weaker species become power saturated before they can be detected. The heterodyne receiver will be described in more detail throughout the rest of the thesis.

The heterodyne receiver used throughout this thesis uses 15 μW of power. To calculate the power, we first looked at a graph of a small scan in which one scan was completed with full attenuation and another scan was completed without attenuation. Attenuation was placed in

between the source and the detector to reduce the power that was being received by the heterodyne receiver. From the graph (Figure 6), you can see the red line (no attenuation) is approximately four times larger than the black (full attenuation). Therefore, the attenuation provides a factor of four to the power leaving the source. To calculate the power being received by the heterodyne receiver a spectrum analyzer was used. The spectrum analyzer was used to check the power (dBm) on the detector side through the first amplifier, both with and without attenuation.

First, the result with attenuation will be considered. The power coming from the radiation source was recorded at point A on Figure 8, and was -11.21 dBm. Next, removing the gains and losses associated with the sub harmonic mixer and the amplifier also seen on Figure 8. The amplifier has a gain of +13.93 dB which results in a final power of -25.14 dBm. The sub-harmonic mixer conversion loss is 7 dB which results in a power of -18.14 dBm. Converting dBm to μW yields a power of roughly 15 μW. Next, the results with no attenuation will be considered. The power coming from the source, at point A on Figure 8, with no attenuation was -2.2 dBm. Subtracting off the gain from the amplifier yields a power of -16.13 dBm. The sub harmonic mixer has a loss of 7 dB resulting in a final power of -9.13 dBm. -9.13 dBm in mW is 122 μW. Now using the two calculated powers, (with (15 μW) and without (122 μW) attenuation) to analyze the affect of attenuation on the power entering the receiver, the attenuation decreases the power by one eighth. Graphically, we saw that the attenuation looked to be about four (Figure 9), but when calculated with the spectrum analyzer it is about 8. This variation is created by nonlinearity within the detector. The nonlinearity creates a minor decrease in the overall sensitivity but does not affect the overall intensity linearity for small absorption features. For future research, including breath analysis, we have attempted to minimize the nonlinearity effect of the detector by removing an amplifier thus limiting the power. The minimal effect of removing an amplifier can be seen in Figure 10.

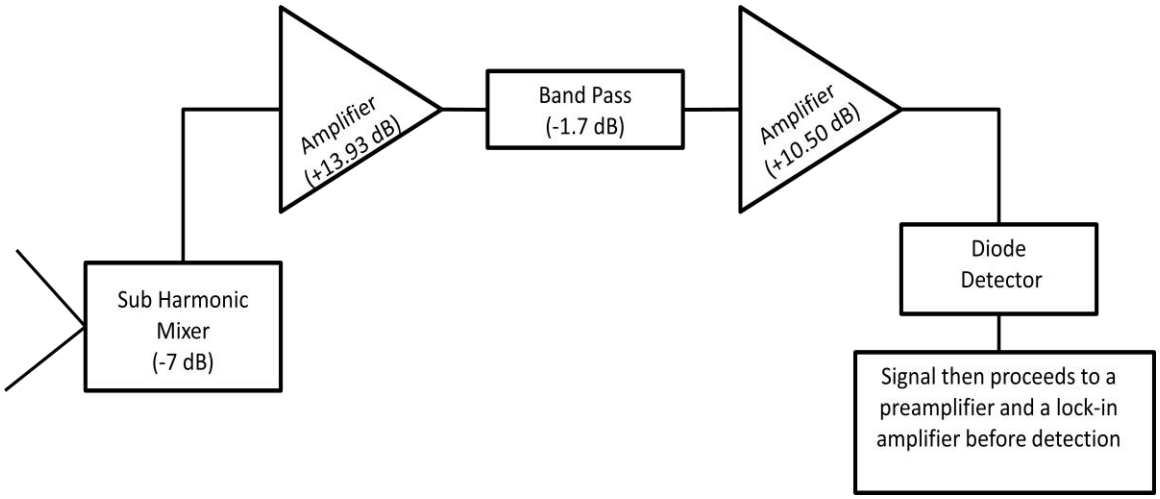

Figure 8 : Diagram of the electronics of the receiver with associated gains and losses.

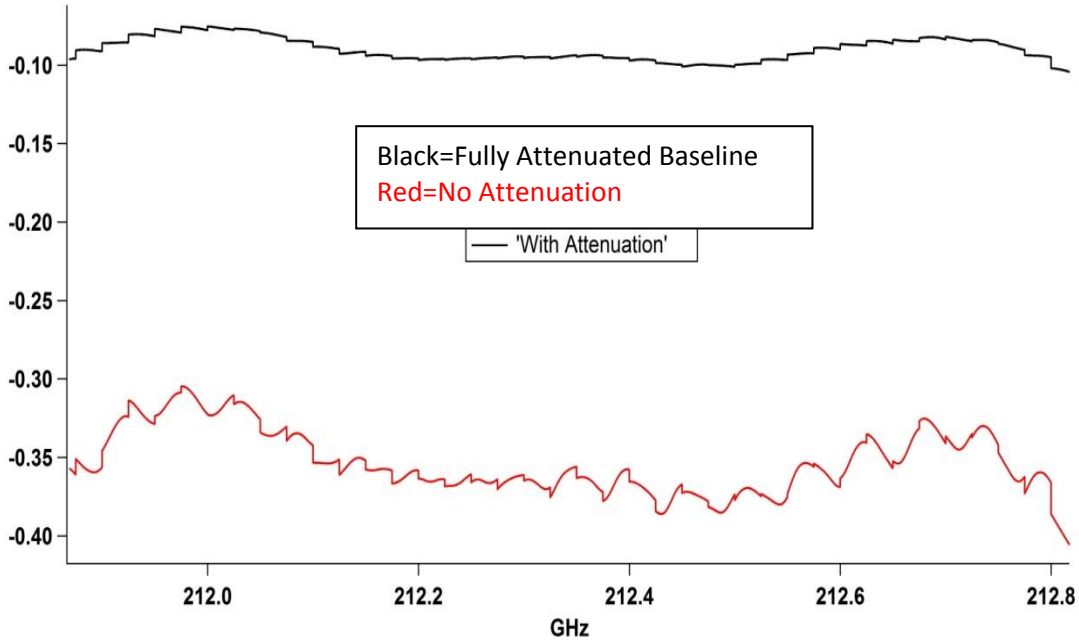

Figure 9 : Graph of a short span of frequency with full attenuation and with no attenuation.

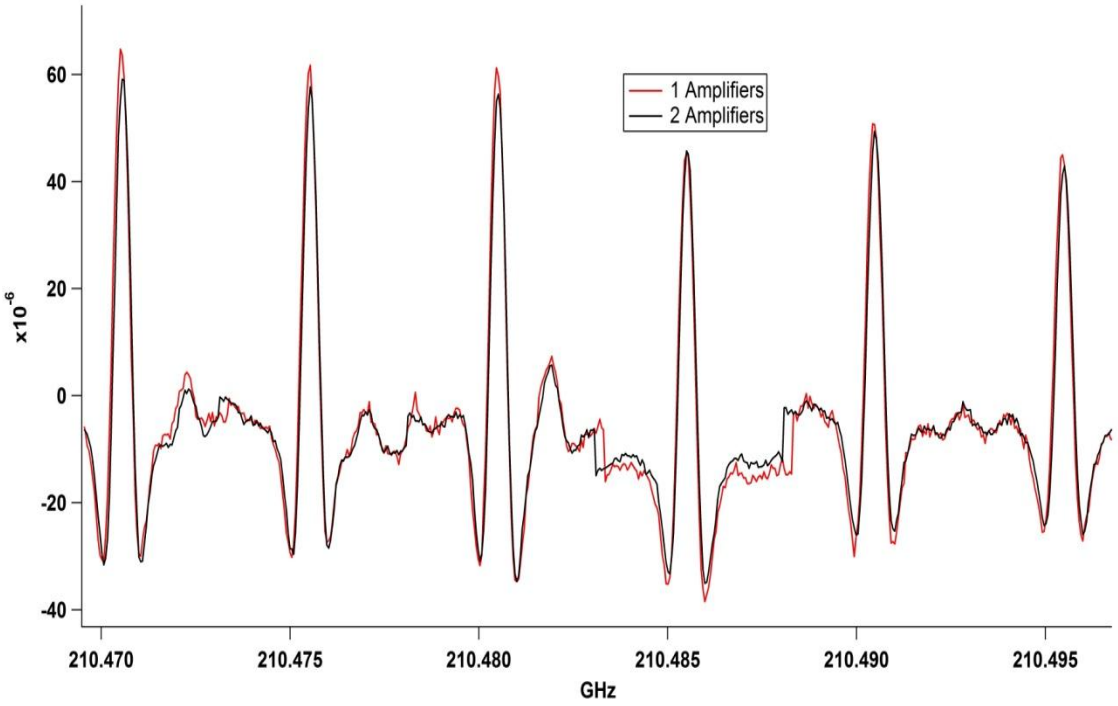

Figure 10 : Spectra of 1 and 2 amplifiers setup to analyze if the amplifier was compressing the signal.

2.2 Degassing and Pressure Control

The cell was coated with SilcoNert 2000 in attempt to speed –up degassing characteristics, which helps prevent the threat of contamination between analytes. SilcoNert 2000 is a surface treatment that prevents surface absorption of analytes. The cell was also maintained at a steady 60℃ to help with the degassing process.

The pressure inside our absorption cell is maintained using a MKS Instruments 600 series pressure controller which works in conjunction with an MKS 120AA Baratron. The 120AA Baratron has range up to 100 mTorr and has an accuracy of 0.12% of the measured pressure. For our sensor, which normally operates at 1 mTorr, the Baratron has accuracy of 0.0012 mTorr. To compare for accuracy and for pressure over 100 mTorr, we also have an MKS Type 626 Baratron pressure transducer which has range from 1 mTorr to 2 Torr and an accuracy of 0.2 mTorr.

2.3 Custom Built Synthesizer

A microwave synthesizer was custom built for this chemical sensor. Following the diagram in Figure 11, the custom synthesizer begins at the rubidium clock. The rubidium clock provides a highly accurate 10 MHz output source. From there, the radiation proceeds in two different paths. The first path is to the Phasematrix FSW-0020 Microwave Synthesizer (B marked in Figure 11). It is a microwave synthesizer that possesses a combination of fast switching and low phase-noise characteristics. It can cover frequency ranges from 0.5 GHz to 20 GHz [19]. The Phasematrix synthesizer (B) was tuned from 8.75 to 11.25 GHz. The signal then proceeds to a power splitter which sends one 10 GHz signal to the VDI receiver which has diodes that multiply the input frequency by twenty-four. The multiplication then puts the frequency into the 210-270 GHz range, which serves as the local oscillator for the heterodyne system. The other branch of the power splitter sends a 10 GHz signal to the mixer. The other path coming from the rubidium clock proceeds to the Herley PCRO Phase Lock Oscillator (A marked in Figure 11), which phase locks 10 MHz reference with its 1 GHz output [20]. The Analog Devices 9910 Synthesizer (C marked in Figure 11) is a direct digital synthesizer (DDS) which includes a 14-bit Digital to Analog Convertor (DAC). It can support sample rates up to 1 Giga Sample per Second (GSPS). The combination of DDS and DAC allows it to be programmed digitally and work with a high frequency. The analog output of the 9910 synthesizer is capable of generating a sinusoidal wave at frequencies up to 400 MHz [21]. The AD9910 (C) provides us with offsets from the 10 GHz frequency, which then mixes with the 10 GHz signal coming from the Phasematrix Synthesizer (B). The AD9910 also has the ability for frequency and amplitude modulation. Once the signals are mixed, meaning there is a center frequency with sidebands, the signal is then sent to the Micro Lambda Wireless YIG filter (D marked in Figure 11). The YIG filter allows us to select one of the side bands created by the AD9910(C) – in our measurements the lower side band was kept. The signal is then sent into the VDI source, which uses diodes to multiply the

frequency by twenty-four. The resulting signal is then sent through the absorption cell and collected by the heterodyne receiver. The heterodyne receiver then mixes the collected signal with the LO signal. The signal then proceeds through an intermediate frequency (IF) chain which is centered at 2.5 GHz. The signal from the IF chain is then rectified by the diode and then demodulated with a lock-in amplifier. The lock-in amplifier provides the ability to record 2f (2nd derivative) lineshapes. The 2f lineshape will be used throughout this thesis (Figure 12), and it allows for the center frequencies of the spectral lines to be determined more easily. The 2f lineshape is the derivative of the 1f line shape. The 1f lineshape is approximately the derivative of the DC spectra and the 2f lineshape is approximately the curvature of the DC lineshape.

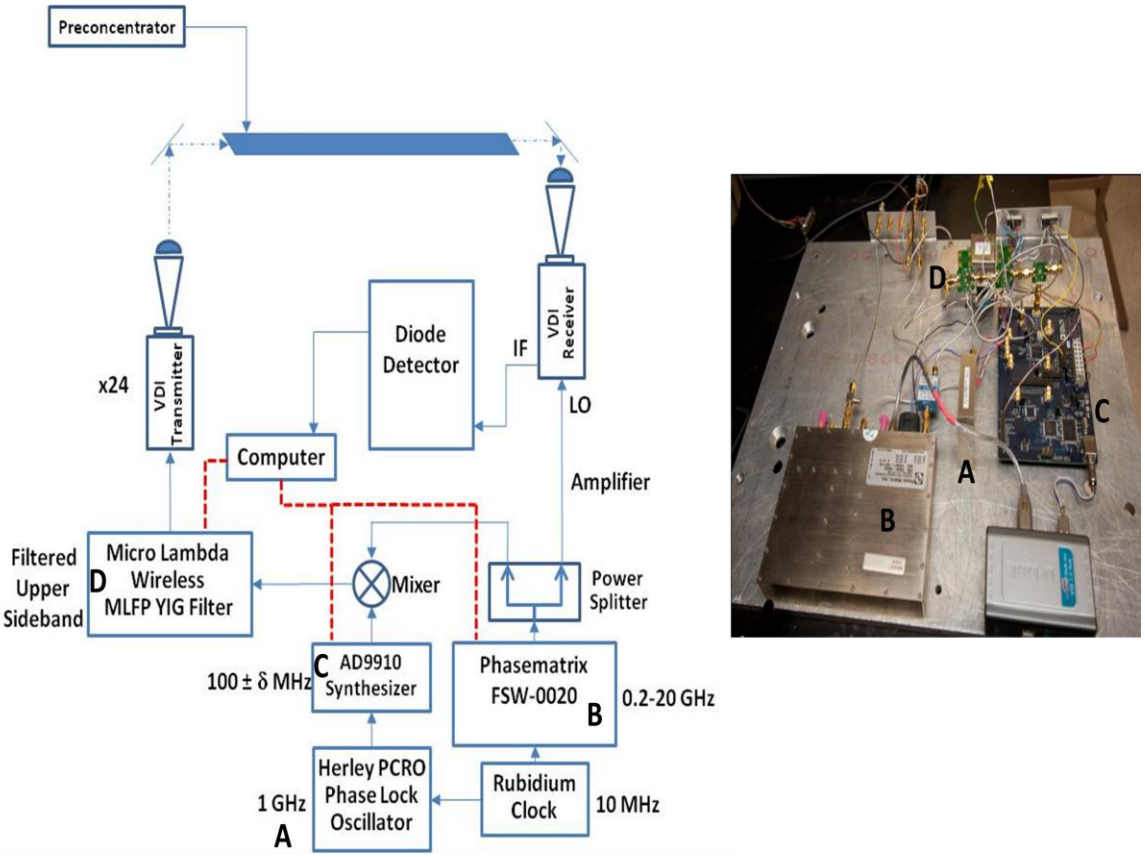

Figure 11 : Custom-built High Frequency Synthesizer.

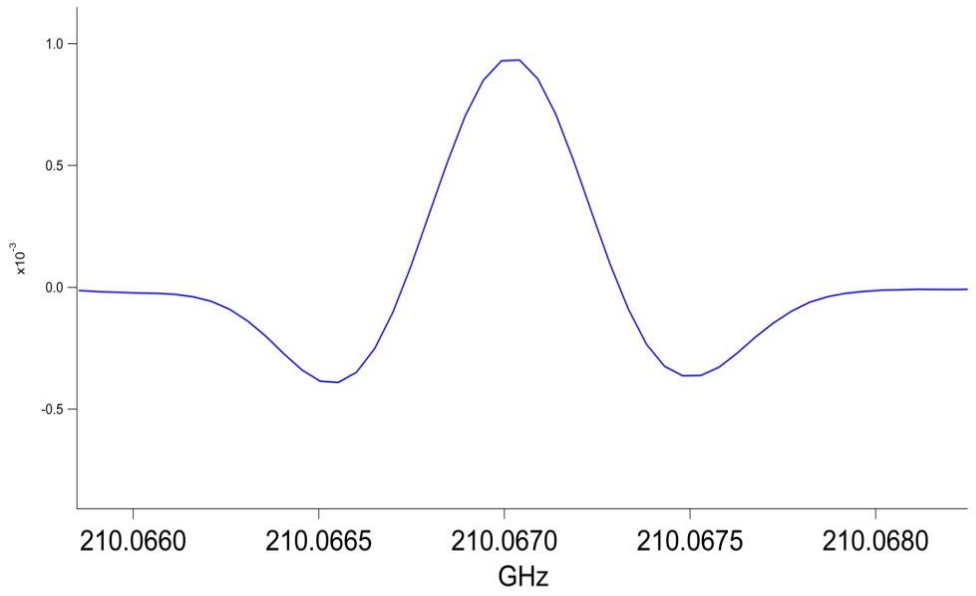

Figure 12 : Example of the 2f spectral lines seen throughout this entire thesis.

2.4 Chemical Selection

A T0-14A mixture was purchased from Scott Specialty Gases and is a certified mixture of thirty-nine volatile organic compounds (VOCs) which are diluted to 1 ppm in nitrogen gas [22]. T0-14A is a calibration standard that is generally used for GC-MS instrumentation. The preconcentrator (Entech 7100A) that was used in this experiment was designed to be used with either GC or GC-MS instrumentation, and therefore the preconcentrator has a high efficiency with the TO-14A Mixture. From the thirty-nine VOCs in the T0-14A mixture, twenty-six VOCs were determined to be suitable for terahertz spectroscopic detection because they have rotational spectra. To determine which polar molecules in the TO-14A mixture had strong rotational spectra; two ab-initio software programs were used. GAMESS [23] and Gaussian [24] were used to calculate the electric dipole moments and the molecular structure of each of the chemicals. The rotational constants for all selected analytes and dipole moments for some of the analytes are shown in Table 2. The dipole moments for all of the analytes are not shown because for the analytes that are composed of heavier molecules GAMESS and Guassian did not return any data. The missing dipole moments could not be located in peer-reviewed literature either. Also,

nineteen of the twenty-six chemicals are on the Clean Air Act of 1990 as hazardous air pollutants [25]. All VOCs in the T0-14A mixture can be seen in Table 1. All selected VOCs can be seen in red and all VOCs on the Clean Air Act of 1990 are asterisked.

Table 1 : All 39 VOCs in TO-14 Mixture.

*Benzene	1,2 Dichlorobenzene	*Cis-1,3 Dichloropropene
*Bromomethane	1,3 Dichlorobenzene	*Trans-1,3 Dichloroethene
*Carbon Tetrachloride	1,4 Dichlorobenzene	*Ethylbenzene
*Chlorobenzene	*1,1 Dichloroethane	*Trichlorofluoromethane
*Chloroethane	1,2 Dichloroethane	*Dichlorodifluoromethane
*Chloroform	1,1 Dichloroethene	*1,1,2-Trichlorotrifluoroethane
*Chloromethane	Cis-1,2 Dichloroethene	*1,2 Dichlorotetrafluoroethane
*1,2 Dibromoethane	*1,2 Dichloropropane	*Hexachloro-1,3 Butadiene
* Methylene Chloride	*Styrene	*1,1,2,2 Tertachloroethane
*1,2,4 Trichlorobenzene	1,1,1 Trichloroethane	*1,1,2 Trichloroethane
1,2,4 Trimethylbenzene	1,3,5 Trimethylbenzene	*Tetrachloroethane
*Toluene	*Trichloroethylene	*Vinyl Chloride
*m-Xylene	*o-Xylene	*p-Xylene

Table 2 : Dipole Moments and A, B, C Rotational Constants for all 26 VOC's.

Dipole Moments & Rotational Constants of Each Chemical									
Chemical	Dipole	A	B	C	**Chemical**	Dipole	A	B	C
Bromomethane	1.80	157.23	9.65	9.65	Freon 114	N/A	2.19	1.14	1.02
Chlorobenzene	1.72	5.69	1.56	1.22	1,2 Dichlorobenzene	N/A	1.87	1.43	0.81
Chloroethane	2.06	31.51	5.34	4.85	1,3 Dichlorobenzene	N/A	2.81	0.85	0.65
Chloroform	1.40	3.28	3.28	1.70	1,1 Dichloroethane	N/A	6.16	3.11	2.19
Chloromethane	1.869	156.72	12.99	12.99	1,2 Dichloroethane	N/A	29.13	1.47	1.42
1,2 Dibromoethane	2.52	5.76	1.51	1.21	1,1 Dichloroethene	1.30	7.39	3.32	2.29
Methylene Chloride	1.60	32.16	3.19	2.96	Cis-1,2 Dichloroethene	1.90	11.62	2.42	2.00
1,2,4 Trichlorobenzene	N/A	1.82	0.59	0.45	1,2 Dichloropropane	3.43	4.64	2.05	1.50
Toluene	0.36	5.73	2.40	1.65	1,1,1 Trichloroethane	N/A	2.29	2.29	1.66
Cis-trans-1,3 Dichloropropene	N/A	12.59	1.09	1.01	1,1,2,2 Tertachloroethane	N/A	1.72	1.09	0.93
Freon 11	0.46	2.41	2.41	1.67	1,1,2 Trichloroethane	N/A	3.43	1.44	1.05
Freon 12	0.51	3.80	2.52	2.11	Vinyl Chloride	1.44	57.56	5.90	5.35
Freon 113	0.80	1.60	1.12	0.91	Trichloroethylene	N/A	3.92	1.49	1.08

2.5 Experimental Strategy

The detection of the twenty-six analytes in the mixture consisted of three main steps. The first step was the creation of spectral libraries. This consisted of collecting spectra of the pure

sample of each analyte at 1 mTorr. Then from the spectra of each analyte, several of the strongest lines were selected to use as markers (snippets) or "fingerprints" for each analyte. Using these markers, a total snippet library was created which contained all of the snippets for all analytes listed continuously in a data file so they could be scanned with the software. The snippets were then scanned consecutively at chosen pressures 0.5,1, 2, and 5 mTorr and were used to check the linearity between the various pressures as can be seen in Section 2.7 Linearity of Intensity.

The next step was the preconcentration phase. In this step a Tedlar bag was filled with 1 ppm of T0-14A mixture. The Tedlar bag ensures that the mixture is at 1 atmosphere (atm) of pressure. From the Tedlar bag the mixture was injected into the preconcentrator, which removes the major air constituents such as H_2O, CO_2, N_2, O_2, and Ar. The preconcentrated mixture is then injected into the absorption cell and the data is recorded using the snippets used for libraries.

The last step was to perform spectral analysis with the mixture that was recorded. To do spectral analysis, a least squares fitting routine (LSQ) was performed. The LSQ returned the partial pressure of each analyte by fitting the mixture spectra to the library spectra. From the partial pressure of each analyte, it is possible to calculate the dilution of each analyte in the mixture or the preconcentration efficiency. The next few sections will go through these three processes in a more in-depth fashion.

2.6 Library Creation

All twenty-six chemicals chosen from the T0-14A mixture were placed into glass flasks and were frozen using liquid nitrogen in attempt to remove air in the head space of each flask that was created from transferring the analytes. Each frozen chemical was separately connected to the vacuum port and evacuated to remove air. Once the air was removed each analyte was separately released into the absorption cell. An overview spectrum was then taken for each chemical from 210 to 270 GHz and at a pressure of 1 mTorr (Figure 13). Each spectrum had the gains adjusted

appropriately to prevent any amplitude saturation that may occur for chemicals that have strong dipole moments. Care was also taken to make sure experimentally specific parameters were appropriate and would yield the best signal to noise possible. These parameters included: post detection band pass, modulation frequency (400 kHz), attenuation (one piece of Plexiglas and one piece of glass ~ a factor of 8), and gains. The band pass filter was set with a preamplifier, which was also used for adjustment of gains. The modulation frequency was set in the software package and 400 kHz was selected because, after experimentation, it provided spectral lines with the highest intensity and spectral resolution. 400 kHz is also within the Doppler linewidth which is essential for frequency modulation, because the modulation frequency must be less than the linewidth for the highest intensity spectral lines. The time constant was set using an external lock-in amplifier; this value has to be set to a time slower than the integration time (software) to prevent spectral lines from becoming asymmetric. To attenuate, glass and Plexiglas were used to limit the power and to remove some of the standing waves present within the absorption cell. The combination of glass and Plexiglas reduces the power going through the absorption cell by a factor of 8. This reduced the power from roughly 100 μw to 12.5 μW. In attempt to gain sensitivity in the less intense spectra, gains had to be adjusted. These experimental parameters were all adjusted to settings which would yield us the best signal to noise, line shape, and the capability to scan the spectrum as efficiently as possible to prevent pressure broadening and chemical deterioration.

Once all the spectrums had been collected with appropriate parameter settings, all spectra were then over-laid using Wavemetric's Igor Pro [26](Figure 14). Also, Igor Pro was used to do an absolute power calibration with each spectrum. The absolute power calibration required normalizing for gains, dividing out the baseline (Figure 15), and subtracting the power of sensor that remains when the sensor's power source is turned off.

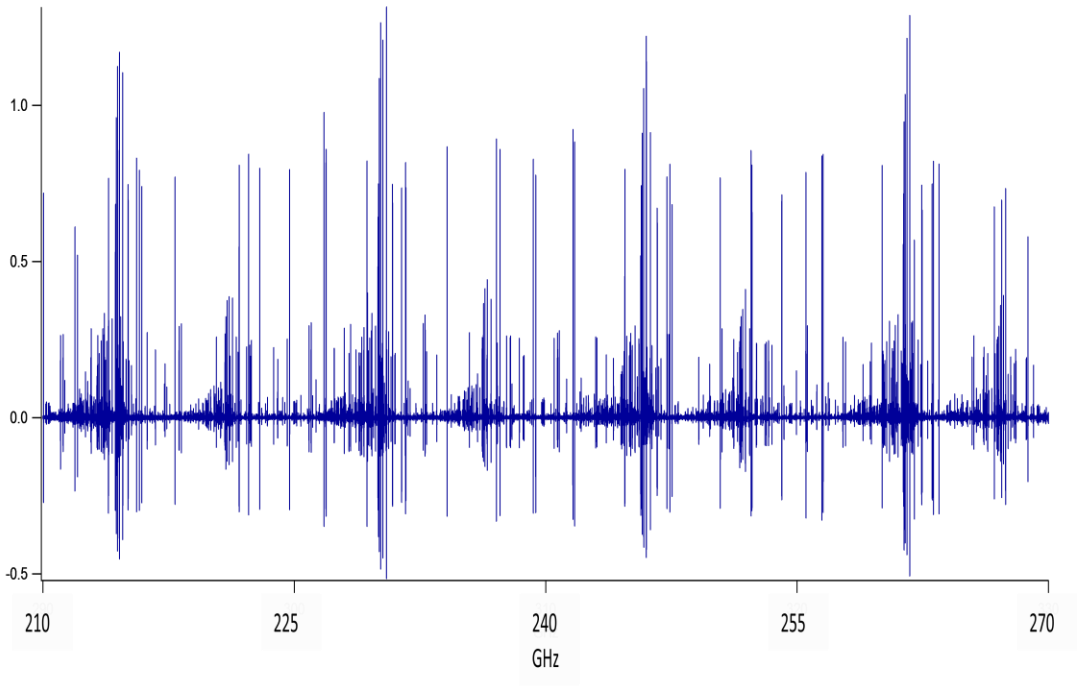

Figure 13 : Overview Spectra of Chloroethane

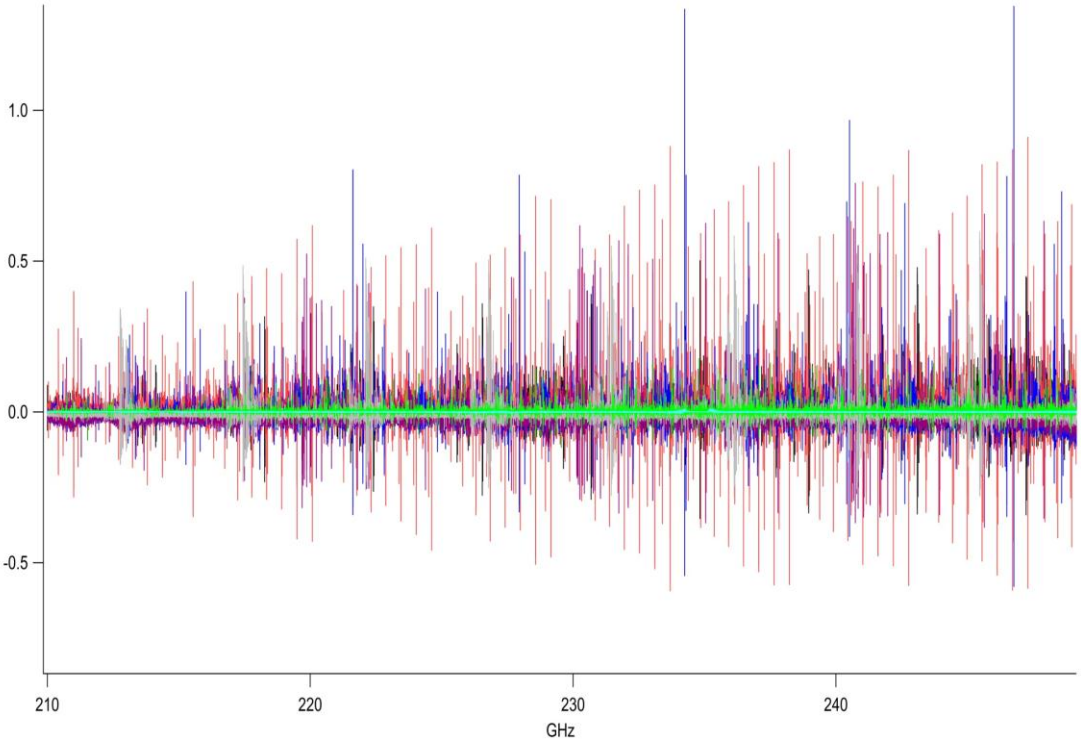

Figure 14 : Overlaying of all 26 chemicals in the standard from 210 GHz to 270 GHz

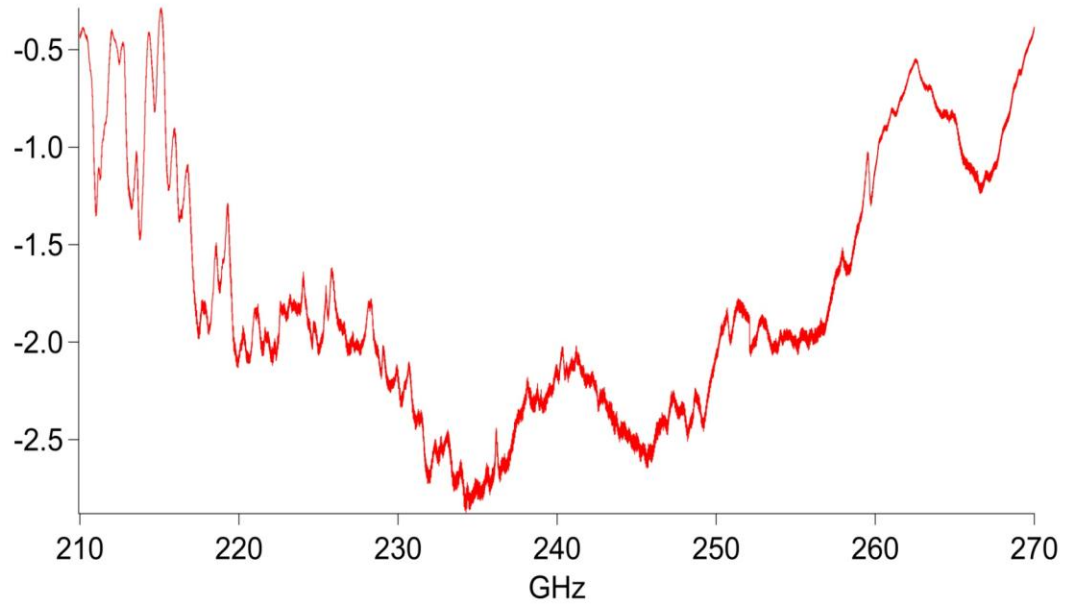

Figure 15 : DC baseline, which was also collected by scan from 210-270 without any sample in the absorption cell.

With all overview spectra now complete, a library of snippets was created. A snippet is a scan around a single line in the spectrum. For each chemical, six to ten lines were selected from within the overview spectrum of each chemical, which showed no overlaps with other chemicals. Now using the spectrometer software, which has a built-in process for dealing with snippets, each snippet was input and a 5 MHz sweep around each line was set up (Figure 16). After making snippets for all twenty-six chemicals, there were a total of 220 snippets. The program allows us to scan all 220 snippets consecutively. Before scanning each chemical, a scan of the DC baseline and power off were recorded for intensity calibration purposes. Using the collection of snippets all twenty-six chemicals were rescanned to ensure that there were no direct overlaps between chemicals were occurring and to create a snippet library (Figure 17). The snippet library spectra were taken at 1, 2 and 5 mTorr. These three distinct pressures were taken so that a linearity check could be performed (described further in the next paragraph).

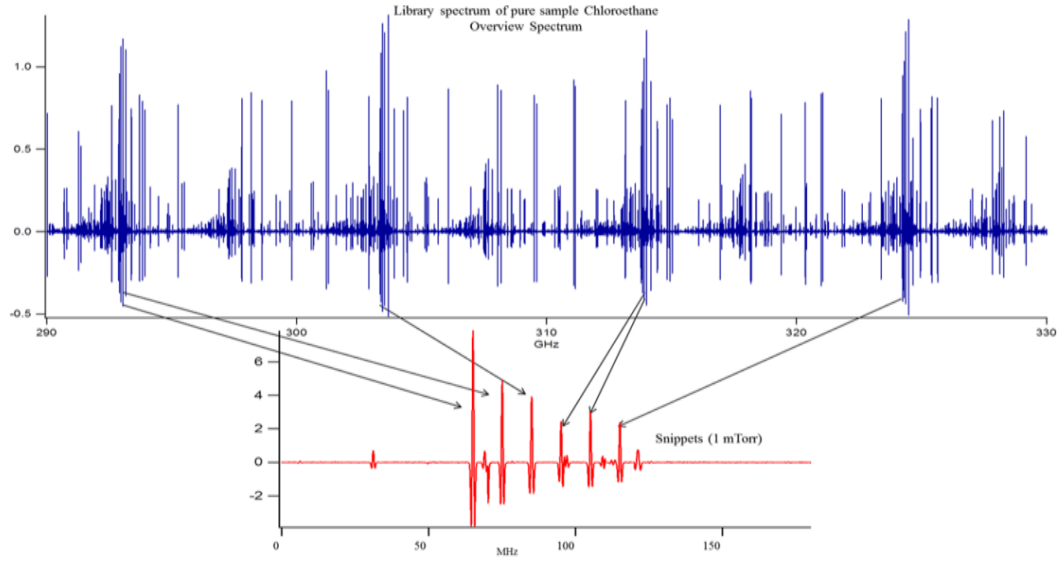

Figure 16 : Snippet selection for Chloroethane

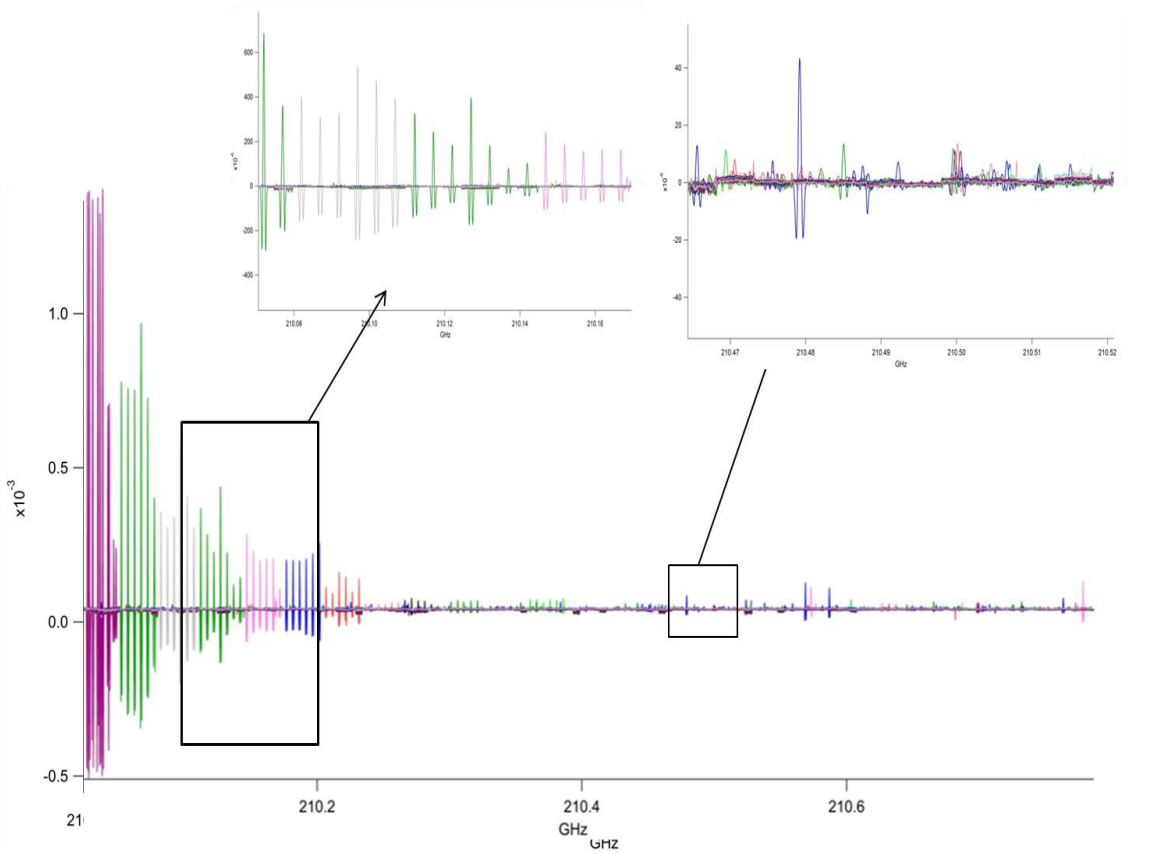

Figure 17 : Overlay of snippet spectrums. Top Left is a zoomed in look at some stronger species. Top right is a zoomed in look at weaker species notice the chemical overlaps that can be seen.

2.7 Linearity of Intensity

A linearity of intensity check was performed using three to four distinctly different pressures. Three different pressures 1 mTorr, 2 mTorr, and 5 mTorr were scanned for each of the analytes. For several of the stronger species, a 0.5 mTorr scan was also taken; this scan was not possible for all chemicals because the weaker chemicals are much more difficult to detect at lower pressures. By overlaying the various pressures and normalizing (dividing out the baseline) for the varying pressure, it was found that the majority of the chemicals would pressure broaden at 5 mTorr. Also, in some of the stronger chemicals, pressure broadening occurs at 2 mTorr and slightly at 1 mTorr, as seen on the left in Figure 18. Figure 18 shows the overlaying of various pressures for two specific chemicals with pressure normalized spectral lines. On the left is Bromomethane, one of the stronger VOCs in which pressure broadening can be seen in the 1, 2, and 5 mTorr spectra. On the right is 1, 1, 1 trichloroethane which shows good linearity amongst the 1, 2 and 5 mTorr spectra. In order to get the highest quality lines and best signal to noise ratio, it was decided that using 2 mTorr and 5 mTorr would diminish our line quality so they were avoided for the final library spectra. 1 mTorr was selected for the snippet libraries even though there still seemed to be some pressure broadening in the stronger analytes. Using less than 0.5 mTorr would not produce high quality spectral lines in many of the weaker species, so 1 mTorr was the selected pressure for all of the libraries.

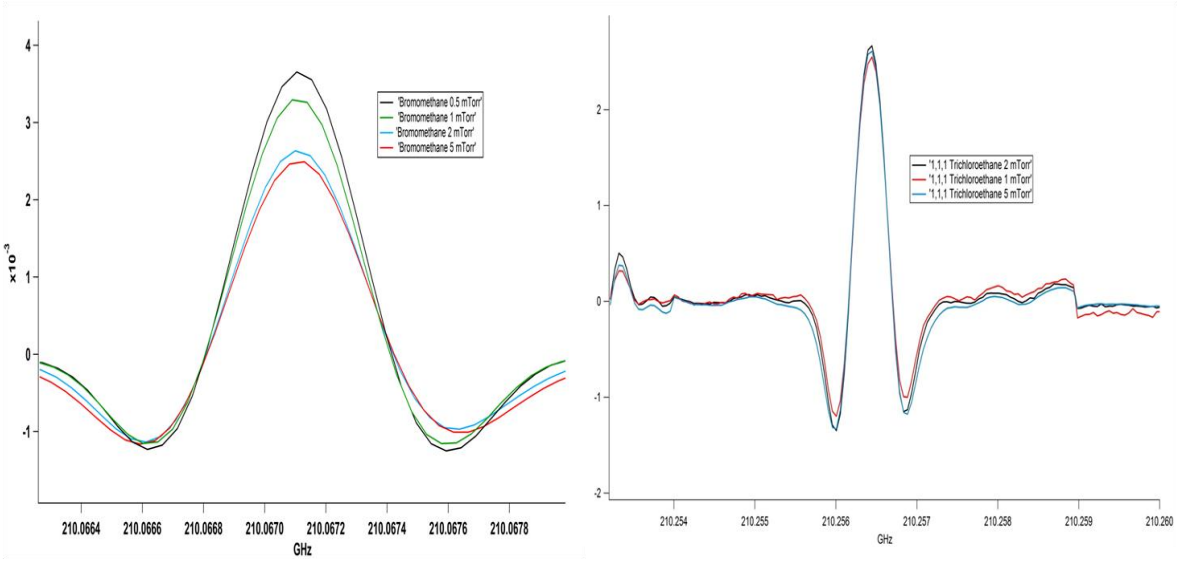

Figure 18 : Left: Compares linearity of 0.5, 1, 2, and 5 mTorr Bromomethane. Right: Compares 1, 2, 5 mTorr of 1, 1, 1 Trichloroethane.

2.8 Preconcentration

Preconcentration was done using an Entech 7100A preconcentrator [27]. The Entech 7100A is a dual stage cryo-sorbent preconcentration system. The preconcentrator uses heating, cooling (liquid nitrogen) and sorbents to eliminate common air constituents such as: oxygen, nitrogen, argon, and carbon dioxide. The two stages the preconcentrator contains are called traps or Module 1 (M1) and Module 2 (M2) (Figure 20) [27]. The preconcentrator has two sampling options. One is "Micro-scale Purge and Trap" (MPT). In this mode, the chemicals go through Module 1(glass beads) at (-150℃) and then are desorbed at (10℃) so that any water will remain frozen in Module 1. The sample is then flushed with helium to move it to Module 2 (glass beads or Tenax) which removes the rest of the air constituents. The other sampling option is "Cold Trap Dehydration" (CTD). In this mode, Module 1 (empty) dehydrates the sample by freezing (-40℃) it, thus removing any water that may be present. The sample is then moved to Module 2 (glass beads) where the preconcentrator freezes (-150℃) the sample and removes the rest of the air constituents. The preconcentrator then evacuates the headspace in M1 and M2 so that it can now be heated (10℃) and release the chemicals into the absorption cell. Experiments were run

using both options, MPT and CTD, but for the final data only MPT was used. MPT was chosen after experimentation with both MPT and CTD. Experimentation with MPT showed recovery of a greater number of analytes compared to CTD. This recovery was also confirmed by Entech, which claims MPT has the highest efficiency rate of the two methods for the TO-14A mixture.

Figure 19 : The Entech 7100A Preconcentrator

The preconcentration cycle begins with filling a Tedlar Bag purchased from Zefon International [28] with the T0-14A mixture that was purchased from Scott Specialty Gases. Each chemical had approximately a 1 ppm dilution in the T0-14A mix. The Tedlar bags were used to ensure that our inlet pressure to the preconcentrator was exactly 1 atmosphere. Using the "Micro-scale Purge and Trap" option, the mixture is ingested from the Tedlar bag at a rate of 75 cc/min. Upon ingestion the sample goes into M1, which has glass beads and freezes and dehydrates (-150℃) the sample. The glass beads provide us with a greater surface area to trap the sample. Once the sample is frozen, the air constituents are then pumped out of the preconcentrator. Then the sample is transferred into M2 at a rate of 10 cc/min. In M2, which has glass beads, it again freezes (-150℃) the sample. The preconcentrator then evacuates the head space over M1 and M2 to prevent pressure broadening and to prepare for sample injection. Then M1 is heated (10℃) and M2 is heated (160℃) for desorption. The sample is injected into our absorption cell, and then using the software the 220 snippets were scanned.

Two scans were completed, one scan with all of the snippets and another scan which only contained the weaker chemicals. The weaker chemicals were scanned separately in an attempt to increase the signal to noise in those snippets. To increase the signal to noise we used a longer integration time and higher gains. If all the snippets are included in the scan, the weaker chemical snippets' signal-to-noise ratio decreases and their spectral lines become difficult to view. This occurs because the stronger chemical snippets' signal is so strong that they experience saturation before the gains can be adjusted appropriately to see the weaker spectra. An example of the resulting mixture can be seen in Figure 21.

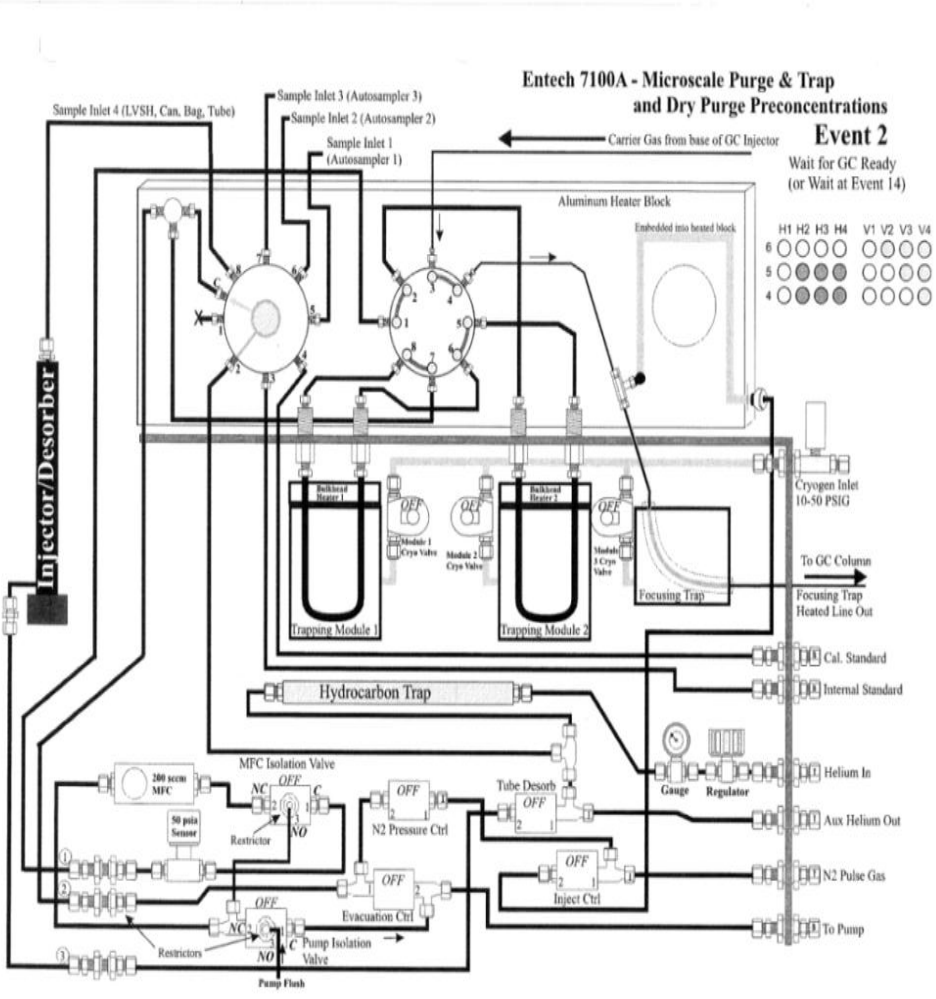

Figure 20 : Inside view of the Entech 7100A Preconcentrator.

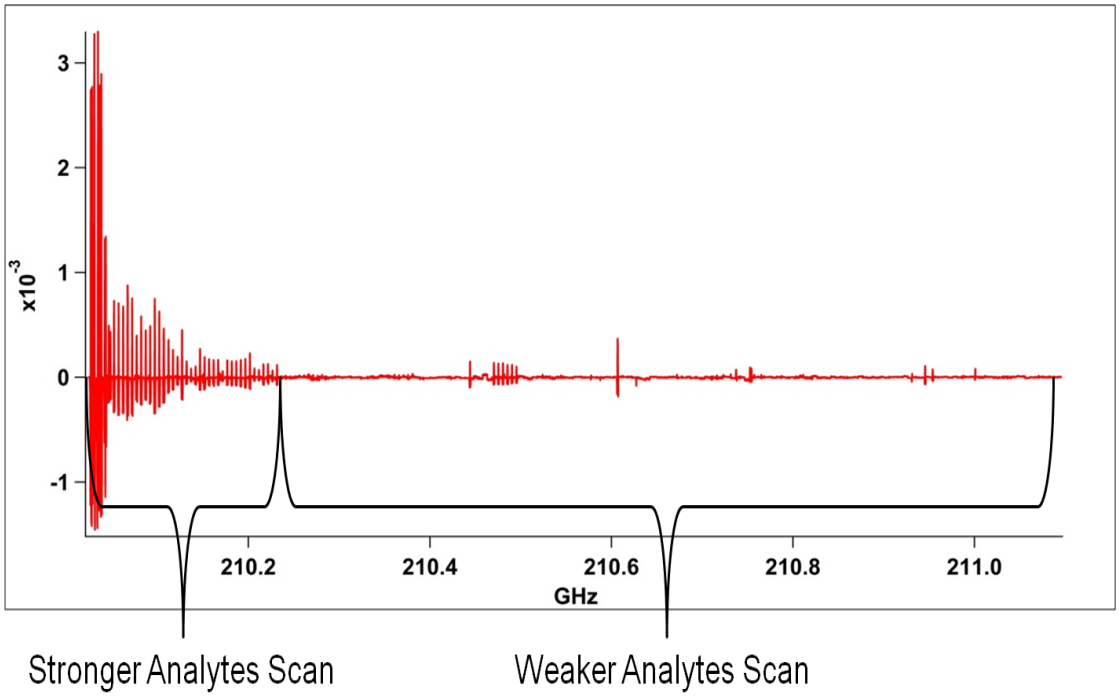

Figure 21 : Mixture of 4500cc of T0-14A

2.9 Spectral Analysis

To perform spectral analysis, a least squares fitting (LSQ) routine was performed on the mixture spectra. The LSQ fitting consisted of fitting for the baseline (440 parameters) and the the intensity of each analytes snippets (26 parameters). The mixture spectra that were used for the LSQ fitting routine were stitched together mixtures that were a combination of the scans that were taken for the stronger and weaker analytes and can be seen in Figure 21. Using the stitched together mixture and the LSQ fitting routine, it is then possible to return the partial pressure of each analyte in the mixture. The partial pressure of each analyte allows for the calculation of either the preconcentration efficiency or the dilution of each analyte in the mixture. The coefficients that were returned by the least squares fit were used in conjunction with Equation 6 to solve for either the dilution of each analyte or the preconcentration effciency.

$$\boldsymbol{Partial\ Pressure\ in\ cell} = (\boldsymbol{ppm})\left(\mathbf{10^{-6}}\right)(\mathbf{760000}\ \boldsymbol{mTorr})\left(\frac{\mathbf{4.5}\boldsymbol{L\ or\ 1L}}{\mathbf{14}\boldsymbol{L}}\right)(\boldsymbol{p}) \qquad \textbf{Equation 6}$$

Now examining Equation 6, the partial pressure in the cell term is the coefficient the least squares fitting routine returns for each chemical. The next term, ppm, is the dilution of each analyte in the mixture in ppm. The next two terms are converting the ingestion pressure of one atmosphere into mTorr. The fourth term is the volumetric dilution; this comes from the fact that our absorption cell has a volume of 14 liters and 4.5 liters of T0-14A mixture was sampled by the preconcentrator. Essentially, what is happening is 4.5 liters is being diluted into 14 liters. The last term in the equation above is the preconcentration efficiency. There are two variables in this formula, which are the chemical dilution within the TO-14A mixture and the preconcentration efficiency for each chemical. To solve for the variables, it is necessary to hold one of them constant and solve for the other. The results of doing this can be seen in Chapter 3.

Chapter 3

3.1 Results

The results of sampling 4500 cc and 1000 cc with a LSQ fitting will be shown in the next few tables (Tables 3-6). Results are shown for glass beads in Module 1 and either glass beads or Tenax in Module 2 of the preconcentrator. Table 3 and Table 4 are the results of sampling 4500 cc with either glass beads or Tenax in Module 2. In all four tables, the expected dilution is the paperwork ppm values provided by Scotts', that came with the purchased TO-14A mixture. The LSQ partial pressure is the partial pressure for each analyte, which were returned from the LSQ fitting routine. The expected partial pressure for each analyte was calculated using the various expected dilutions and Equation 6. The dilution, when the preconcentration efficiency is kept at 100%, was calculated using the LSQ partial pressures for each analyte and solving for the ppm term in Equation 6. It is also possible to return the preconcentration efficiency (p) but it just results in values that are identical to the recovered dilution column. The last column in Table 3 and 4 are the ratio between 1000 cc and 4500 cc for each analytes partial pressure.

First, considering the results of sampling 4500 cc, notice that not all the analytes are shown. Several of the analytes were not recovered effectively so their results are not included in these tables. The entire results of the LSQ fitting for all analytes, which includes the absorption coefficients, error, and S/N, can be seen in Appendix A. First, considering Table 3 for results in which Tenax was used. The percent of dilution that was recovered after preconcentration ranges from 5% to 98%, but for the majority of the recovered analytes range from 40% to 70%. The

mixture of 4500 cc with Tenax returned conclusive results for only fourteen of the twenty-six analytes. The 1000 cc mixture with Tenax in Module 2 also returned fourteen conclusive results. The results that can be seen in Table 4 for glass beads are not as good. The 4500 cc mixture with glass beads returned only seven conclusive results compared to the 1000 cc mixture, which returned eleven conclusive results. There was a much greater overall recovery of all of the analytes when Tenax was used (Table 5). Glass beads struggled with being able to preconcentrate the 4500 cc and 1000cc mixture consistently and results of two preconcentration can be seen in Tables 4 and 5. Glass beads recovered significantly more analytes when only 1000 cc was sampled compared to 4500 cc. This is most likely caused by the glass beads reaching the maximum capacity of mixture that it can effectively trap; examples of this can be seen in Table 3.

Tenax also seem to struggle preconcentrating 4500cc and some of the results in Table 3 and 5 reflect that in the form of diminished dilution recovery percentages (S9, S11, and S13). The main reason Tenax works more effectively is because it uses chemical bonding to absorb the analytes were as with glass beads the sample bonds to the surface of the bead. One important aspect to note can be seen in Table 4, and looking at 1, 2 Dichloroethane (S13). 1,2 Dichloroethane's dilution recovered and preconcentration efficiency both return results that imply that both were over 100%, which is not a accurate result. Any occurrences of over 100% recovery or preconcentration efficiency can be attributed to pressure broadening within the library spectra and is in the process of being resolved.

The 1000 cc mixture on the other hand is not an issue for either glass beads or Tenax, but Tenax did have much better results. Sampling 1000 cc is more ideal for the purpose of this sensor in the long term, because the goal of this sensor is to be able to do breath analysis with a small sample size or exhalation. An average exhalation is approximately 1000 cc; in the long run sticking with sample sizes of 1000cc is in our best interest and the best interest of the

preconcentrator. A sample of 1000cc will be sufficient for spectral analysis, once spectral clutter and the sensitivity of the sensor are better addressed.

Table 3 : Tenax 1000 & 4500 cc samples

Chemical		PPM	Expected Partial Pressure	1000cc LSQ Partial Pressure	Recovered Dilution %	4500cc LSQ Partial Pressure	Recovered Dilution %	Ratio between 4500cc &1000 cc	Freezing Point (℃)
Chloromethane	S2	1.040	0.056	0.054	99.105	0.242	98.948	4.493	-97.7
Bromomethane	S3	0.950	0.052	0.038	69.447	0.172	70.598	4.575	-93.66
Vinyl chloride	S4	1.000	0.054	0.041	76.079	0.193	78.804	4.661	-153.8
Chloroethane	S5	0.970	0.053	0.020	36.842	0.088	36.179	4.419	-139
Methylene Chloride	S6	0.960	0.052	0.017	31.082	0.082	33.719	4.882	-96.7
Cis-1,2-Dichloroethene	S7	1.020	0.055	0.018	33.158	0.083	33.900	4.601	-81
1,1 Dichloroethane	S8	1.000	0.054	0.018	32.697	0.078	31.914	4.392	-97
1,1,1 Trichloroethane	S9	1.000	0.054	0.006	10.211	0.016	6.587	2.903	-33
Chloroform	S10	1.010	0.055	0.005	9.408	0.027	11.127	5.322	-63.5
Chlorobenzene	S11	1.000	0.054	0.016	28.659	0.014	5.616	0.882	-45
1,2 Dichloroethane	S13	1.030	0.056	0.025	46.734	0.079	32.405	3.120	-157.7
Trichloroethylene	S14	1.030	0.056	0.025	45.150	0.173	70.715	7.048	-73
1,2 Dichlorobenzene	S15	1.030	0.056	0.003	5.292	0.022	8.903	7.570	-17
1,1 Dichloroethene	S16	1.000	0.054	0.018	33.211	0.089	36.339	4.924	-122

Table 4 : Glass Beads 1000 & 4500 cc samples.

Chemical		PPM	Expected Partial Pressure	1000 cc LSQ Partial Pressure	Recovered Dilution %	4500 cc LSQ Partial Pressure	Recovered Dilution %	Ratio between 4500cc &1000 cc	Freezing Point (℃)
Chloromethane	**S2**	**1.040**	**0.056**	**0.000**	**0.640**	**0.001**	**0.276**	**1.939**	**-97.7**
Bromomethane	**S3**	**0.950**	**0.052**	**0.001**	**1.970**	**0.001**	**0.396**	**0.905**	**-93.66**
Vinyl chloride	**S4**	**1.000**	**0.054**	**0.001**	**1.194**	**0.001**	**0.269**	**1.013**	**-153.8**
Chloroethane	S5	0.970	0.053	0.018	33.453	N/A	N/A	N/A	-139
Methylene Chloride	S6	0.960	0.052	0.045	82.689	0.006	2.339	0.127	-96.7
Cis-1,2-Dichloroethene	S7	1.020	0.055	0.054	99.185	0.101	41.269	1.872	-81
1,1 Dichloroethane	S8	1.000	0.054	0.047	86.923	0.151	61.892	3.204	-97
1,1,1 Trichloroethane	S9	1.000	0.054	0.050	92.440	0.167	68.341	3.327	-33
Chloroform	S10	1.010	0.055	0.017	31.107	0.071	28.889	4.179	-63.5
Chlorobenzene	S11	1.000	0.054	0.034	62.769	N/A	N/A	N/A	-45
1,2 Dichloroethane	S13	1.030	0.056	0.058	106.461	0.141	57.735	2.440	-157.7
Trichloroethylene	S14	1.030	0.056	0.020	36.460	0.014	5.778	0.713	-73
1,2-Dibromoethane	S19	1.030	0.056	0.005	10.081	N/A	N/A	N/A	10
1,2 Dichlorpropane	S20	1.040	0.056	0.015	28.499	N/A	N/A	N/A	-100

Table 5 : Dilution percent recovery. N/A values mean that the chemical was not recovered.

	Tenax		Glass Beads	
Chemical	1000cc	4500cc	1000 cc	4500 cc
S2	99.105	98.948	0.639	0.275
S3	69.447	70.598	1.969	0.396
S4	76.079	78.807	1.194	0.268
S5	36.842	36.179	33.453	N/A
S6	31.082	33.719	82.688	2.341
S7	33.158	33.899	99.184	41.268
S8	32.697	31.914	86.922	61.892
S9	10.211	6.586	92.439	68.340
S10	9.408	11.126	31.107	28.889
S11	28.659	5.615	62.769	N/A
S13	46.734	32.404	106.460	57.734
S14	45.150	70.715	36.460	5.778
S15	5.292	8.903	N/A	N/A
S16	33.211	36.338	N/A	N/A
S19	N/A	N/A	10.080	N/A
S20	N/A	N/A	28.498	N/A

Lastly if the linearity of the two sample sizes is considered, it will provide insight into the effectiveness of the preconcentrator (last column of Table 3 and 4). The ratios seen in Table 3 and 4 are supposed to be around 4.5 because of the difference between the two mixture sample sizes (1000 and 4500). As you can see for the most part the Tenax ratio hovers around 4.5, any nonlinearity (Figure 23) is likely created by issues with the 4500cc sample that have been previously discussed. The nonlinearity also speaks to not effectively trapping the sample in the glass beads or the Tenax in the 4500cc samples. There are more linearity issues with several of the analytes when glass beads are used. This nonlinearity again was created by the inefficiency of the preconcentrator when using a mixture of 4500 cc and the overall inconsistency of the preconcentrator when working with glass beads-glass beads. From the results of looking at the

linearity it is plausible to say that Tenax is definitely more effective and consistent than just glass beads and should be used moving forward.

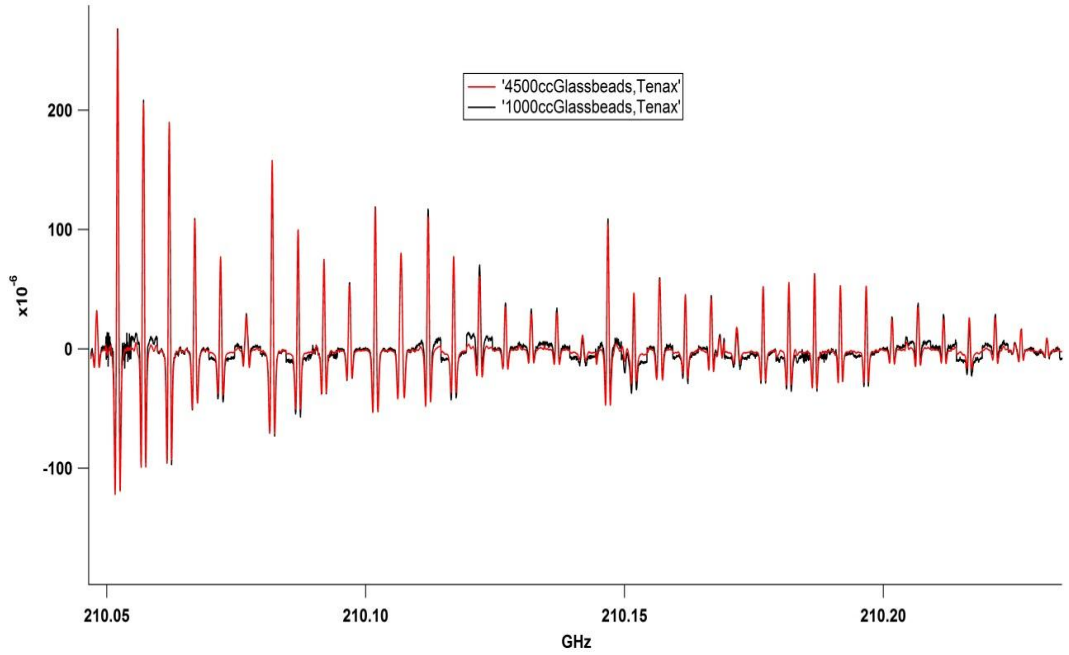

Figure 22 : 2 Tenax samples normalized for sample size in order to examine linearity.

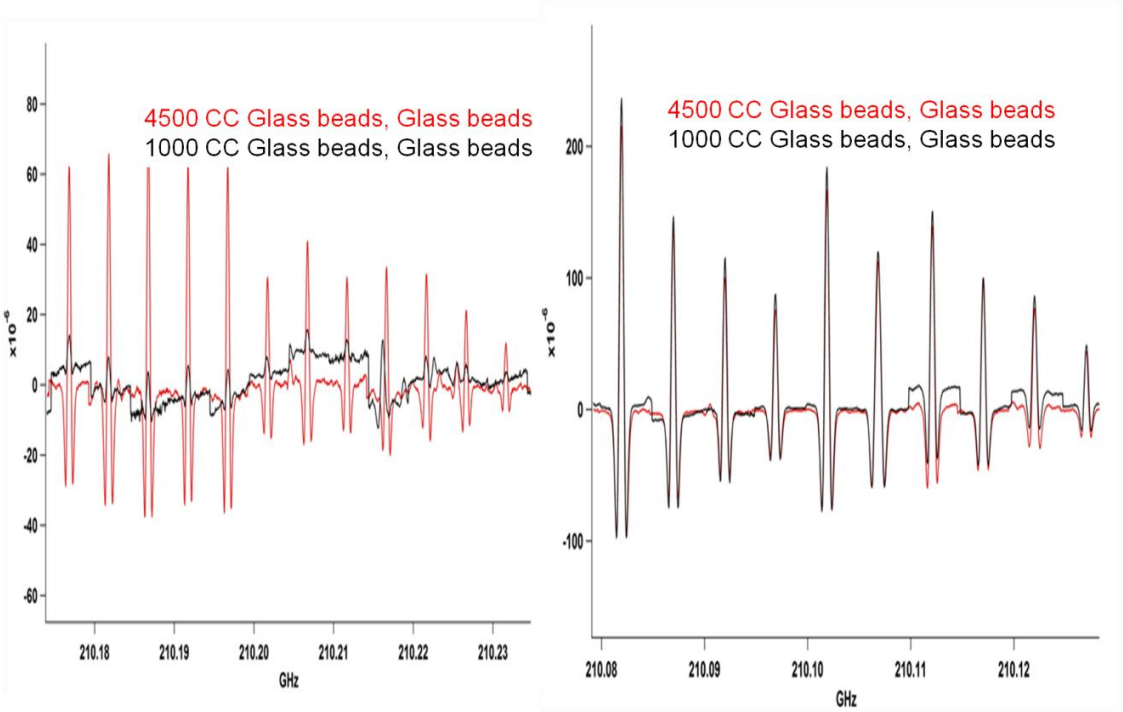

Figure 23 : 2 Glass bead (4500cc & 1000cc) samples normalized for sample size in order to examine linearity. On the left is a section of the mixture that is not linear. On the right is a linear section.

3.2 Spectral Clutter

Spectral clutter is another aspect of chemical mixture analysis that must be considered. Clutter has been shown to be a limiting factor for atmospheric gas sensors in other frequency ranges mainly the optical/infrared (OP/IR) [28]. Again, noting that our sensor is Doppler limited and pressure broadening effects are minimal, the effects of atmospheric clutter are not as severe as what is seen in the OP/IR [28]. This is because the Doppler widths in the THz region are 100-1000 times smaller than what is seen in other spectral regions. Other factors to consider are atmospherically abundant molecules, such as H_2O, have strong spectra in the OP/IR, but hardly any notable spectral lines in the THz region [28]. Our sensor is also highly accurate with frequencies and uses an intensity calibration, which also limits the effects of clutter in the spectra.

A graphical exploration of the spectral clutter within twenty-one of the twenty-six selected analytes can be seen in Figure 24 and analysis of the figure in Table 9. Some of the analytes were not included because it was difficult to distinguish the noise floor and the spectral lines from one another in a few of the weaker species. In order to prevent the inclusion of noise of those select few, and because of limited data sets, a few chemicals were left out (1, 1, 2, 2-Tetrachloroethane, Freon 113, Freon 11, Toluene, 1, 3 dichlorobenzene). The four analytes left off the graph are also four of the weakest analytes that were studied, and other than Toluene they were not recovered. Further analyzing Figure 25, the top curve is a summation of all the lines present above the noise floor for each analyte, when an overview scan from 210-270 was completed. Then moving down the graph from the top curve, the rest of the curves correspond to the number of lines in each individual analyte (210-270 GHz) and they follow the order that can be seen in Table 6. To analyze this graph we selected the point on each analytes collection of lines that corresponded to the number of snippets used for each analyte. In Table 6, the number of competing lines column came from selecting the point on the thick red curve(summation of all

analytes), which was horizontally across from the point selected on the curve of number of lines in each individual analyte.

Using the data, from Table 6, a few things can be deduced. First, a couple pieces of important information that are needed are the Doppler linewidth, which over the viewable spectra averages to 0.91 MHz and there were a total of 94,524 lines in the twenty-one chemicals. Using the 94,524 total line and that each line averages a linewidth of 0.91 MHz it can be shown that if all the spectral lines were together they would span about 86 GHz. Remembering that the sensor operates in the 210-270 GHz range, which is only a range of 60 GHz, one might think there could be some foreseeable issues with detecting lines which had no overlaps with other chemicals. This did become an issue with many of the weaker species, which required recreating the snippet library in attempt to eliminate the overlaps. After several attempts to eliminate all of the spectral overlaps there were still issues with the spectral detection of the weaker species.

But, if the clutter is examined on an analyte to analyte basis, you will see that for the majority of the analytes, clutter does not become an issue at the concentrations that we studied. Using the average linewidth of 0.91 MHz, the number of snippets and number of competing lines from Table 6 , it can be shown that the spectral space that is available is sufficient for the majority of the analytes (Table 7). One must also remember that the spectral lines for any given analyte are systematically spaced throughout the spectral range and the minimum spacing between two adjacent lines for the spectral lines to still be detectable is 0.4 MHz.

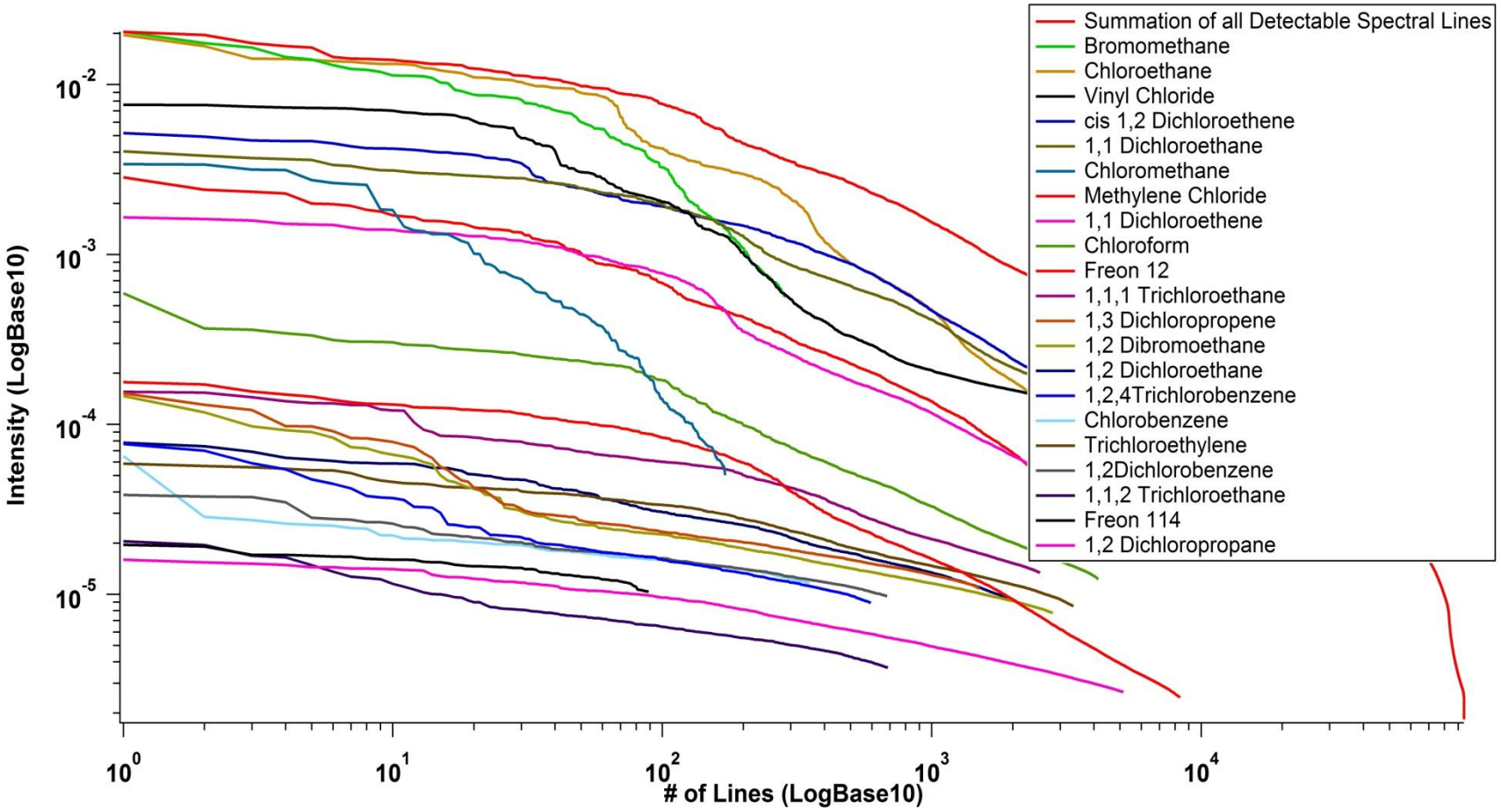

Figure 24 : Top red curve is all lines distinguishable above the noise of 21 of the chemicals sorted by intensity. The rest of the curves are for the 21 chemicals listed in order in Table 7. There are a total of 94524 total lines in the 21 chemicals.

Table 6 : Spectral clutter with the number of lines present of each analyte and the total number of competing lines for each analyte for 21 of 26 chemicals. The number of competing lines value includes all lines above the noise floor.

Chemical	# of Snippets	# of Competing Lines	Chemical	# of Snippets	# of Competing Lines
Bromomethane	6	18	1,3 Dichloropropene	12	34672
Chloroethane	7	12	1,2 Dibromoethane	9	37141
Vinyl Chloride	6	113	1,2 Dichloroethane	6	55893
cis-1,2-Dichloroethene	6	198	1,2,4Trichlorobenzene	16	64435
1,1-Dichloroethane	6	326	Chlorobenzene	13	66591
Chloromethane	5	475	Trichloroethylene	6	64642
Methylene Chloride	6	743	1,2 Dichlorobenzene	10	77483
1,1 Dichloroethene	6	1048	1,1,2 Trichloroethane	14	45687
Chloroform	7	5624	Freon 114	12	70696
Freon 12	6	14977	1,2 Dichloropropane	10	73334
1,1,1, Trichloroethane	6	16295			

Table 7 : The frequency range that the spectral clutter spans at the same intensity level if all the lines were at the minimum separation (0.1 MHz) that allows for detection of adjacent lines.

Chemical	Clutter Span (GHz)	Chemical	Clutter Span (GHz)
S2	0.1900	S13	22.357
S3	0.0072	S14	25.857
S4	0.0452	S15	30.993
S5	0.0048	S16	0.4192
S6	0.2972	S18	18.275
S7	0.0792	S19	14.856
S8	0.1304	S20	29.334
S9	6.5180	S21	13.868
S10	2.2496	S22	25.774
S11	26.636	S23	28.278
S12	5.9908		

Examining a few of the analytes more thoroughly for clutter, Chloromethane (S2) has 5 snippets that were used and a Doppler width within those lines of 0.98 MHz. That means that those 5 spectral lines are competing with spectral clutter that covers 190 MHz of spectral space. 190 MHz of clutter is a small percentage of the available 60 GHz, so it is not going to become an issue in detecting Chloromethane in the mixture that we studied. Next considering a weaker species Trichloroethylene, which has six snippets, is one the analytes that was not recovered. The

six snippets are competing with nearly 26 GHz of spectral clutter. 26 GHz is about half of the viewable spectral area for which the chemical sensor works. Many of the weaker analytes that were not recovered effectively have spectral clutter similar to Trichloroethylene, which covers nearly half of the viewable spectral area and can be seen in Table 7. In many of the weaker analytes, spectral clutter becomes a major factor in the overall ability to detect the spectral signature of the weaker analytes. Another contributing factor to the overall ability to detect analytes is the sensitivity of the sensor.

3.3 Sensitivity

The process of effectively detecting analytes is also affected by the sensitivity of the sensor. The sensor in its current configuration is at a sensitivity of 1 ppb. The sensitivity was calculated from the least squares fitting. One of the values the fitting returns is the averaged signal to noise (S/N)(Table 9), which is just the partial pressures of each analyte (signal) divided by the error in the fit (averaged noise). For the strongest species chloromethane in the 4500cc mixture, LSQ returned a S/N about 10500 to 1. The T0-14A mixture which was ingested by the preconcentrator was a 1 ppm mixture. Therefore, with a S/N of 10500 to 1 at 1 ppm returns a final sensitivity of 0.1 ppb. Chloromethane in the 1000cc mixture returned a S/N of about 2322. A S/N of 2322 corresponds to a sensitivity of about 0.5 ppb. It is interesting to note that the S/N of the two mixtures does scale roughly with the amount sampled (4500cc versus 1000cc). Another way to calculate the sensitivity is to look at the S/N graphically. If we look at it graphically (Figure 25 and Figure 26), we get a S/N of 780 for the 4500cc mixture looking at Chloromethane, which results in about a 1 ppb sensitivity. Comparing the two methods of sensitivity calculation, they differ by one order of magnitude. This occurs because the least squares fitting averages the S/N giving an order of magnitude better.

Table 8 : S/N of 4500cc and 1000cc Mixture of the recovered analytes

Chemical		Tenax		Glass Beads	
		1000cc	4500cc	1000cc	4500 cc
Chloromethane	S2	2322.175	10427.3	14.979	29.04
Bromomethane	S3	474.4775	2168.66	13.4465	12.1741
Vinyl chloride	S4	390.5215	1818.58	6.12385	6.2006
Chloroethane	S5	152.3245	671.455	137.968	N/A
Methylene Chloride	S6	112.9815	551.546	300.573	38.2542
Cis-1,2-Dichloroethene	S7	104.0705	477.481	310.454	581.28
1,1 Dichloroethane	S8	66.4445	291.835	176.634	565.969
1,1,1 Trichloroethane	S9	3.47755	10.0943	31.4816	104.735
Chloroform	S10	12.37665	65.8753	40.9255	171.033
Chlorobenzene	S11	18.96165	16.6953	41.4681	N/A
Freon 12	S12	N/A	21.6561	N/A	N/A
1,2 Dichloroethane	S13	20.371	63.5575	46.4016	113.239
Trichloroethylene	S14	4.57236	32.2177	3.69133	2.63265
1,2 Dichlorobenzene	S15	2.55647	19.3514	0.203264	N/A
1,1 Dichloroethene	S16	32.74935	161.246	9.41534	3.38132
Freon 11	S17	N/A	6.14355	N/A	N/A
1,2-Dibromoethane	S19	15.32615	54.5981	0.989293	N/A
1,2 Dichlorpropane	S20	N/A	N/A	1.64346	N/A
Freon 114	S23	3.06174	32.9221	N/A	N/A
Toluene	S25	11.17885	47.9184	N/A	N/A
Freon 113	S26	N/A	19.2495	N/A	N/A

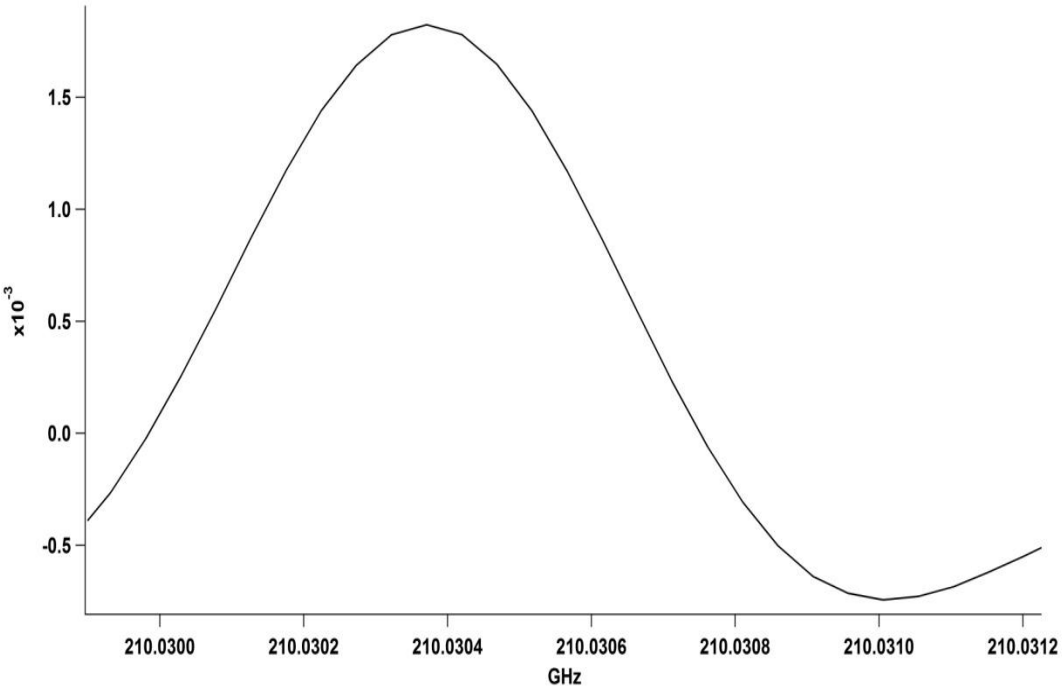

Figure 25 : A spectral line from the chloromethane snippets

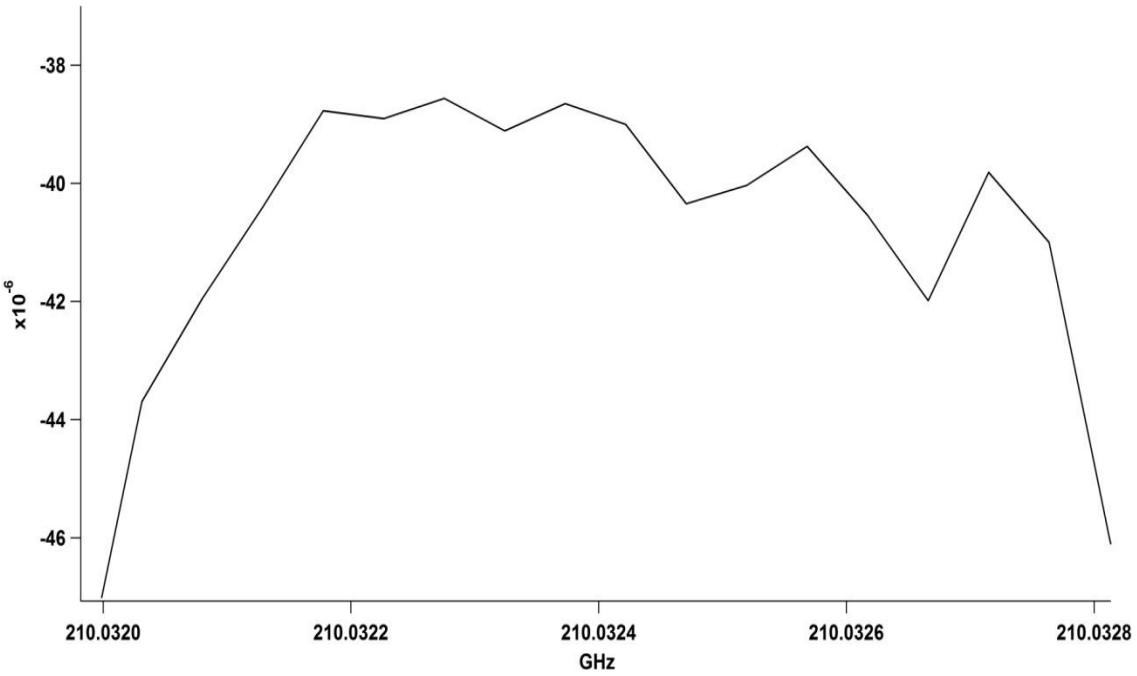

Figure 26 : The noise associated with the spectral line in Figure 25.

There are several ways to improve the sensitivity of the sensor. One way would be to reduce the volume of our absorption cell (14 Liters). In doing this, it would then allow us to reduce the volumetric dilution. Reducing the volumetric dilution would eliminate the factor of 14 from Equation 6, thus improving the sensitivity. The other possibility to increase the sensitivity is increasing the time spent per point. Currently, the sensor waits 18 ms per point. There are 22440 points, so it takes 5 minutes to scan through the snippets once. If the time per point was increased to from 0.018 ms to 1 s that would take 6 hours to do a single scan. Even just increasing the time per point by a factor of 10 to 0.1 s would still take 40 minutes per scan. Therefore, increasing the time per point by even a factor of ten would increase the sensitivity, although it may also create significant issues with chemical deterioration and pressure broadening. Increasing the time per point would be a great idea if we were only focusing on a few chemicals, but since we are working with twenty-six chemicals, it would probably not be in the best interest of the experiment to wait this long.

3.4 Breath Analysis

Throughout this research it has been demonstrated that a THz sensor is capable of analytic chemical sensing for environmental purposes. The sensor can be made more compact and most likely will be in the future. This would be completed by just making an absorption cell with only a 1 liter volume. By decreasing the volume, the sensitivity of the sensor would increase from the ppb range to well into the ppt range. This research also opened the possibility of using the sensor with other complex mixtures and for other applications; mainly exhaled human breath.

One application of interest is exhaled breath analysis. As stated throughout this thesis, we have developed a THz sensor with high specificity and sensitivity. Using our specificity and sensitivity, it is possible to examine a large number of different analytes. Many of the large number of examinable analytes that have a THz spectral signature are exhaled breath constituents. As mentioned previously, a single exhaled breath is approximately 1000cc and our sensor has been shown to have full functionality with a small amount of sample such as 1000cc.

Examining human breath has several applications. The main applications are pre/post symptomatic diagnosis and occupational exposures. Breath analysis would be a non-invasive test compared to the common blood tests or other invasive testing currently being performed. What would happen is a patient would give a sample of his/her breath, using their breath the procedure would follow the description covered in Chapter 2 closely. The only difference would be that a new set of libraries would need to be created using VOCs that are known to be in human breath that are relevant to different injuries/illnesses (Table 12). After library recreation, it would then proceed to preconcentration and then a least squares fitting of the spectra. From the fitting, the concentration of each VOC in the patient's breath would be returned and from that, a possible diagnosis could follow based off what the normal allowed levels (Column 2, Table 12) of each chemical were supposed to be.

Table 9 : VOC's and known illnesses/injury and the concentration found within breath.

VOC	Normal levels(Adults)	Potential Metabolic Disorders/ Diseases
Acetone	177 - 3490 ppb	Lung cancer, dietary fat losses, heart failure, brain seizure, diabetes mellitus, ketonemia
Methanol	32 - 1684 ppb	Nervous system disorder, renal failure, pancreatic insufficiency, carbohydrate malabsorption
Ethanol	0 - 1663 ppb	Production of gut bacteria
Nitric Oxide	7.8 - 41.1 ppb	Asthma, hypertension, lung diseases, air way inflammation, lung inflammation
Carbon Monoxide	0 - 6 ppm	Oxidative stress, respiratory infection, anemia, hyperbilirubina, asthma
Methyl Mercaptan	ABNORMAL: 0.3-0.5 ppm (to produce bad breath)	Halitosis, liver damage
Methylamine		Protein metabolism in body, hepatitis, renal diseases
Ethanolamine		
Nitrous Oxide	1 - 20 ppb	Anesthetics
Nitrogen Dioxide		

Preliminary experimentation has begun on breath analysis using the analytes in Table 9, but mainly focusing on Acetone, Methanol and Ethanol. These VOCs were chosen because they have known spectral lines and are present in human breath. With the selected analytes, snippet libraries were recreated so that breath could be sampled. Next, a sample of breath was donated. The breath was sampled from a Tedlar bag and then preconcentrated following same procedures that were seen in Chapter 2. The initial results showed recovery of acetone, methanol and ethanol (Figure 27). Having the ability to detect acetone and ethanol is already an improvement on current available technologies. The typical breathalyzer that law enforcement uses (attempts to detect ethanol levels in the breath) has difficulties detecting acetone (commonly elevated in humans that have diabetes) and ethanol separately, so there is the potential of returning a false positive. Because our sensor has the capabilities to detect both acetone and ethanol, the first experiment that was conducted was drinking a beer (32 oz 4.2%), so we could see how the intensity of the spectra evolved over time (Figure 28). In Table 13 and Figure 29 the evolution over time is shown. The ethanol levels seem to peak at about one hour and forty minutes after the beer was drank and then decays from there, which is what was to be expected. The second

experiment that has been conducted was eating fruit in attempt to elevate acetone levels. Acetone is commonly present in breath from eating different foods and especially fruits (ketonemia) [31]. To do this experiment two oranges an apple and a banana were eaten. The results of this can be seen in Table 14 and Figure 30. It seemed as though the acetone levels peaked at about an hour after the fruit was consumed and then decayed from there. The acetone level taking an hour to peak speaks to the time it takes for the fruit to metabolize in the stomach. The experimentation is in trial two now and both prior experiments will be repeated with better accuracy for future review.

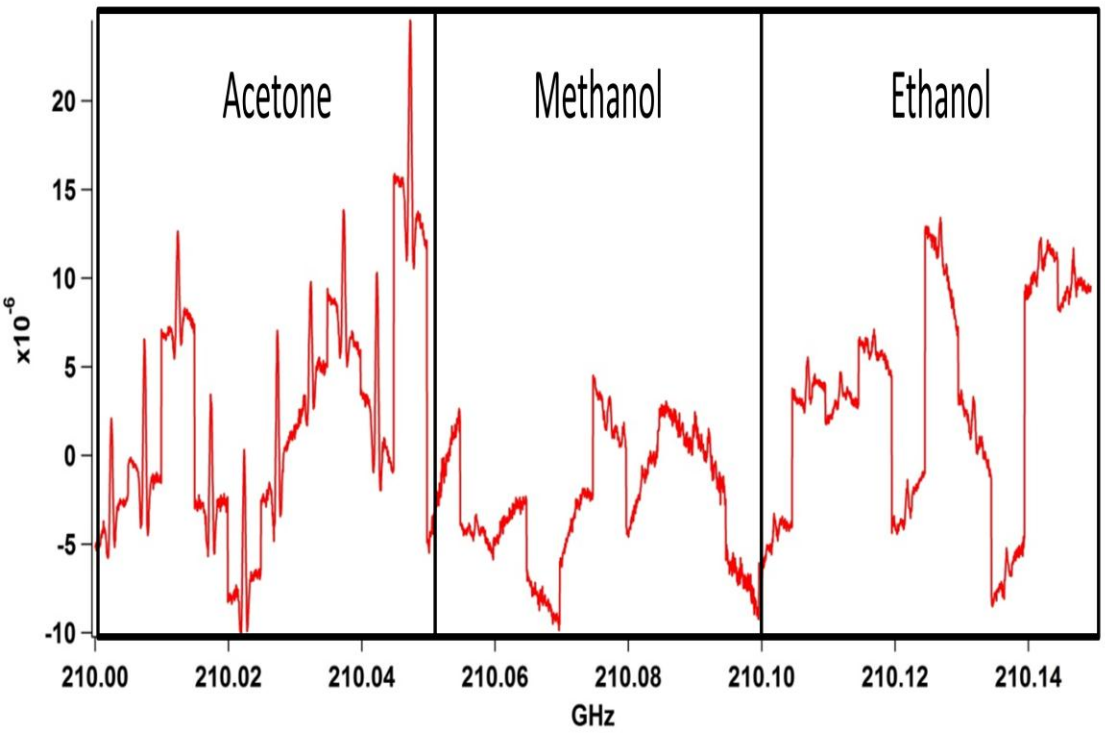

Figure 27 : Typical breath sample with Acetone, Methanol, Ethanol. The jumps in the graph are from using snippets. The snippets sweep 5 MHz around each selected spectral line, and each spectral line may be in a different region of the available spectrum.

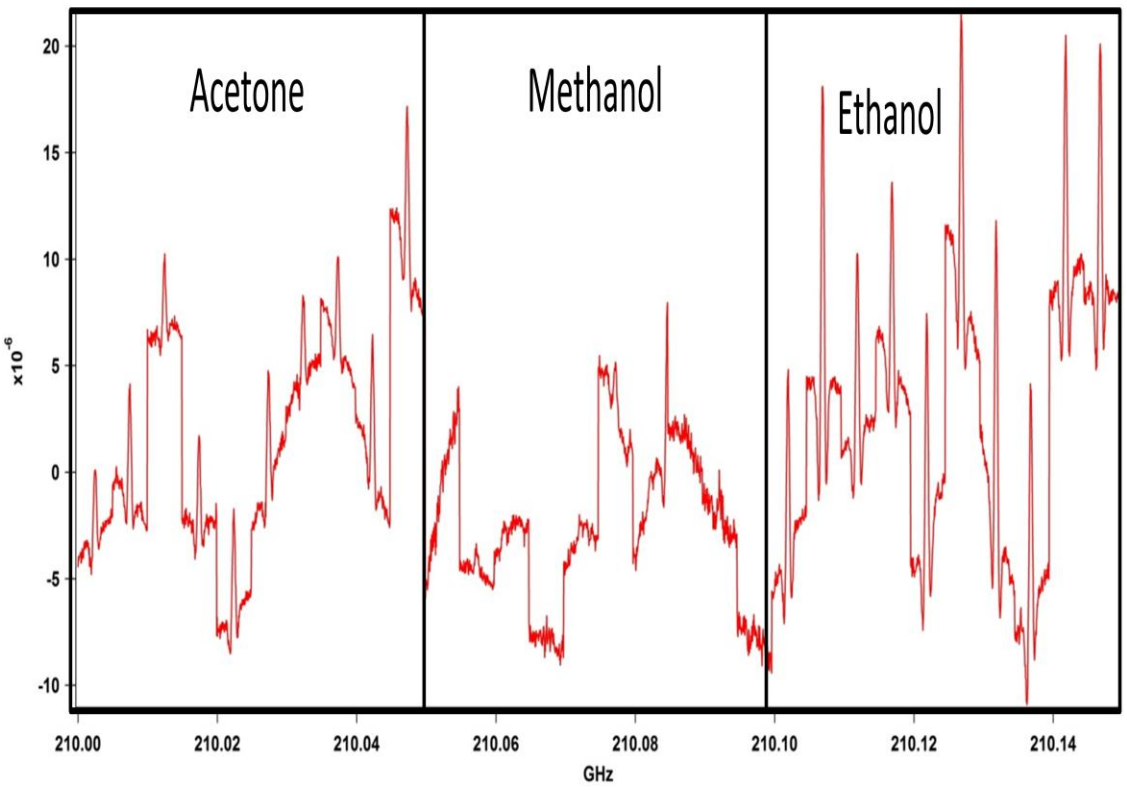

Figure 28 : Sample of my breath after a beer. The jumps in the graph are from using snippets. The snippets sweep 5 MHz around each selected spectral line, and each spectral line may be in a different region of the available spectrum.

Table 10 : Intensity levels of the spectra over 10 time intervals after and before drinking a beer.

The Beer Experiment			
Time (Beer)	Acetone(ppm)	Methanol(ppm)	Ethanol(ppm)
-164	5.683712	0.638224	1.337942
-49	3.271698	0.48848	0.30552
10	2.373744	0	67.63567
67	1.910827	0.1924	119.8827
97	2.308165	0.457056	92.61561
122	0.560701	0.065136	62.54891
149	0.567773	0.131072	58.45141
200	4.615405	0.944672	46.40594
230	3.505237	0.74304	10.20608
270	3.650458	0.766592	5.616818

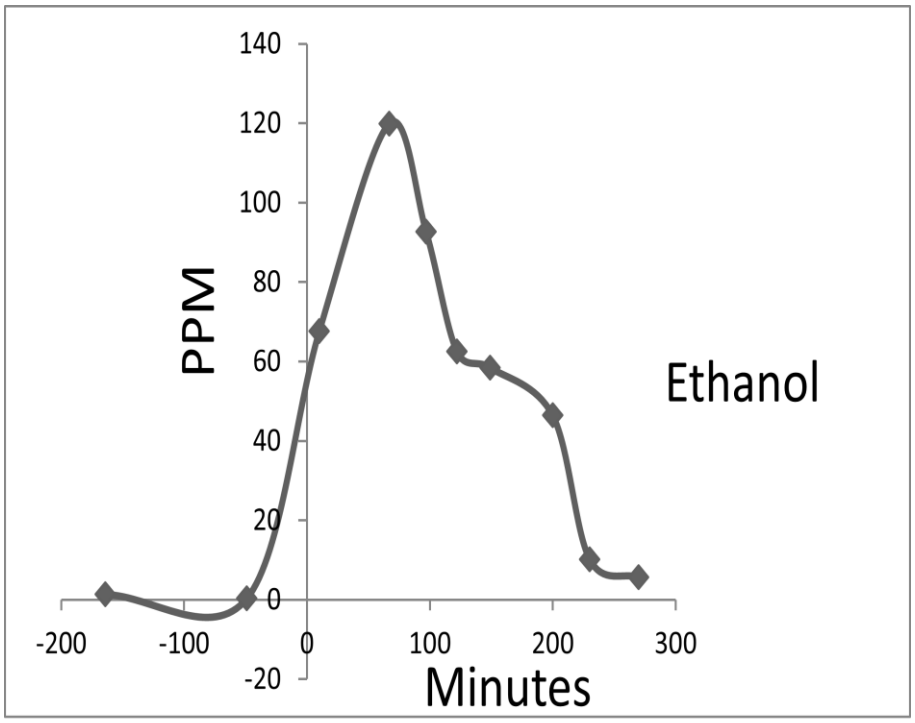

Figure 29 : Evolution of Ethanol intensity levels over time.

Table 11 : Intensity levels of the spectra over 7 time intervals after and before eating fruit.

The Fruit Experiment			
Time (Fruit)	Acetone	Methanol	Ethanol
-38	0.368859	0.023981	0.029100
-2	0.412954	0.022664	0.034084
54	0.556189	0.097866	0.088894
89	0.407569	0.047555	0.040097
155	0.324474	0.051612	0.013473
224	0.065125	0.017537	0.002586
274	0.493078	0.094238	0.008792

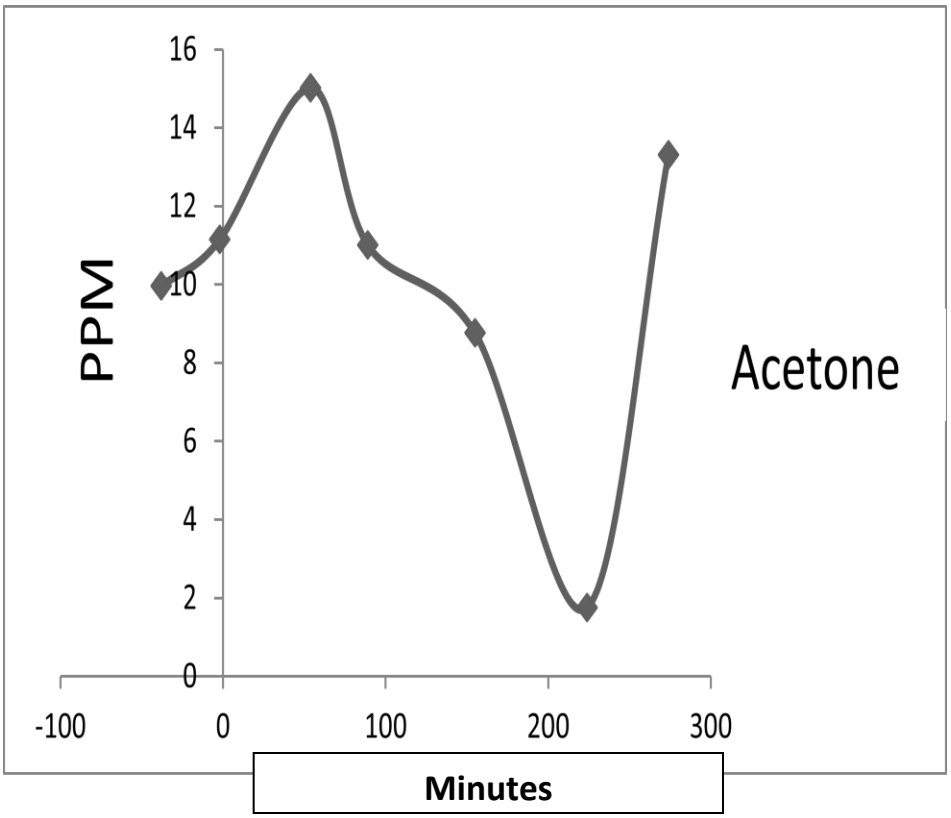

Figure 30 : Evolution of Acetone intensity levels over time after eating fruit.

Appendix A

Below, complete LSQ results for Glass Beads, Tenax sampling 4500cc and 1000cc are shown. S/N with a negative sign means that the results are inconclusive, so only results with positive S/N and a value over 1 were kept.

Tenax		1000cc			4500cc		
Chemical		Partial Pressure	S/N	Error	Partial Pressure	S/N	Error
Chloromethane	S2	0.053837	4644.35	2.31836E-05	0.241717	10427.3	2.31812E-05
Bromomethane	S3	0.037721	948.955	7.94999E-05	0.172461	2168.66	7.95242E-05
Vinyl chloride	S4	0.041313	781.043	0.000105788	0.192507	1818.58	0.000105856
Chloroethane	S5	0.020049	304.649	0.00013162	0.088381	671.455	0.000131626
Methylene Chloride	S6	0.016873	225.963	0.000149346	0.082371	551.546	0.000149346
Cis-1,2-Dichloroethene	S7	0.018045	208.141	0.000173387	0.082812	477.481	0.000173435
1,1 Dichloroethane	S8	0.01775	132.889	0.000267139	0.077962	291.835	0.000267144
1,1,1 Trichloroethane	S9	0.005543	6.9551	0.00159397	0.01609	10.0943	0.00159401
Chloroform	S10	0.005107	24.7533	0.000412622	0.027182	65.8753	0.000412621
Chlorobenzene	S11	0.015576	37.9233	0.000821464	0.013719	16.6953	0.000821703
Freon 12	S12	-0.02354	-17.6989	0.00265974	0.066089	21.6561	0.00305174
1,2 Dichloroethane	S13	0.02537	40.742	0.00124541	0.07916	63.5575	0.00124549
Trichloroethylene	S14	0.02451	9.14472	0.00536054	0.172747	32.2177	0.00536186
1,2 Dichlorobenzene	S15	0.002873	5.11294	0.00112381	0.021749	19.3514	0.0011239
1,1 Dichloroethene	S16	0.018029	65.4987	0.000550508	0.08877	161.246	0.000550525
Freon 11	S17	-0.03724	-9.69888	0.00767857	0.047177	6.14355	0.00767908
1,1,2 Trichloroethane	S18	-0.11876	-38.2829	0.00620407	-0.48722	-78.5209	0.006205
1,2-Dibromoethane	S19	0.084786	30.6523	0.0055321	0.302018	54.5981	0.00553166
1,2 Dichlorpropane	S20	-0.0561	-11.9185	0.00941375	-0.21765	-23.1212	0.00941352
1,3 Dichloropropene	S21	-0.05197	-13.9057	0.00747456	-0.12902	-17.2559	0.00747656
1,2,4 Trichlorobenzene	S22	-0.0364	-5.67783	0.0128217	-0.47834	-37.293	0.0128266
Freon 114	S23	0.040099	6.12348	0.0130968	0.432438	32.9221	0.0131352
1,3 Dichlorobenzene	S24	-0.07769	-25.6527	0.00605709	-0.57495	-94.9202	0.00605719
Toluene	S25	0.131672	22.3577	0.0117786	0.564528	47.9184	0.011781
Freon 113	S26	-0.06017	-9.28706	0.0129573	0.249582	19.2495	0.0129656
1,1,2,2 Tetrachloroethane	S27	-0.18713	-32.3904	0.0115546	-1.33118	-115.197	0.0115557

Glass Beads		1000cc Glass			4500		
Chemical		Partial Pressure	S/N	Error	Partial Pressure	S/N	Error
Chloromethane	S2	0.000347	14.979	2.32E-05	0.000673	29.04	2.32E-05
Bromomethane	S3	0.001069	13.4465	7.95E-05	0.000968	12.1741	7.95E-05
Vinyl chloride	S4	0.000648	6.12385	0.000105856	0.000656	6.2006	0.000105856
Chloroethane	S5	0.01816	137.968	0.000131626	-0.0075	-57.0112	0.000131626
Methylene Chloride	S6	0.044888	300.573	0.000149342	0.005713	38.2542	0.000149346
Cis-1,2-Dichloroethene	S7	0.053843	310.454	0.000173434	0.100814	581.28	0.000173434
1,1 Dichloroethane	S8	0.047187	176.634	0.000267143	0.151194	565.969	0.000267143
1,1,1 Trichloroethane	S9	0.050182	31.4816	0.00159399	0.166947	104.735	0.001594
Chloroform	S10	0.016887	40.9255	0.000412626	0.070572	171.033	0.000412621
Chlorobenzene	S11	0.034075	41.4681	0.000821709	-0.0029	-3.52324	0.000821711
Freon 12	S12	-0.00176	-0.57546	0.00305179	-0.0067	-2.19549	0.00305178
1,2 Dichloroethane	S13	0.057793	46.4016	0.00124549	0.141038	113.239	0.00124549
Trichloroethylene	S14	0.019793	3.69133	0.00536194	0.014116	2.63265	0.00536178
1,2 Dichlorobenzene	S15	0.000228	0.203264	0.00112391	-0.00309	-2.74513	0.00112392
1,1 Dichloroethene	S16	0.005183	9.41534	0.000550528	0.001862	3.38132	0.000550525
Freon 11	S17	-0.02146	-2.79482	0.00767896	-0.01562	-2.03457	0.00767889
1,1,2 Trichloroethane	S18	0.000416	0.067017	0.00620483	-0.03968	-6.39558	0.0062049
1,2-Dibromoethane	S19	0.005473	0.989293	0.00553172	-0.0099	-1.78986	0.00553166
1,2 Dichlorpropane	S20	0.015471	1.64346	0.00941347	-0.0202	-2.14564	0.00941349
1,3 Dichloropropene	S21	-0.00755	-1.0107	0.00747435	-0.04249	-5.68379	0.00747647
1,2,4 Trichlorobenzene	S22	0.003649	0.284439	0.0128271	-0.0635	-4.9501	0.0128271
Freon 114	S23	-0.00156	-0.11842	0.0131356	-0.02712	-2.06436	0.0131355
1,3 Dichlorobenzene	S24	-0.01943	-3.20705	0.00605715	-0.04653	-7.68203	0.00605712
Toluene	S25	-0.04774	-4.05238	0.0117808	-0.03837	-3.25689	0.0117811
Freon 113	S26	-0.02995	-2.30965	0.0129657	-0.04917	-3.7923	0.0129655
1,1,2,2 Tetrachloroethane	S27	0.011412	0.987513	0.0115561	-0.00081	-0.06973	0.0115555

Appendix B

Minimum sample size calculation with volume of 1liter, at a pressure of 1 mTorr, an absolute power of 100% and a S/N of $10^7 \frac{1}{\sqrt{Hz}}$

$$\frac{1L}{10^7} = 10^{-7} mTorr$$

Now converting pressure to Pascal

$$10^{-7} mTorr = 10^{-7} mTorr \cdot \frac{0.133\ Pa}{1\ mTorr} = 1.33 \cdot 10^{-8} Pa$$

Lastly using the ideal gas law and solving the number of mols (N).

$$N = \frac{pV}{RT} = \frac{(10^{-8} Pa)(10^{-3} m^3)}{8.31 \frac{J}{mol \cdot K} \cdot 300K} = 4 femtomoles$$

For a typical analyte such as chloromethane with a molar mass of 50.49 $\frac{g}{mol}$ the minimum sample size is then:

$$= 4 femtomoles \cdot 50.49\ \frac{g}{mol} = 201.96 \text{ femtograms}$$

Bibliography

[1] J. A. Seeley, "Early Warning Chemical Sensing," *Lincoln Laboratory Journal*, vol. 17, no. 1, pp. 85-99, 2007.

[2] M. Atashbar, S. Krishnamurthy and G. Korotcenkov, "Basic Principles of Chemical Senosor Operation," in *Chemical Sensors: Fundamentals of Sensing Materials*, New York, Momentum Press, 2010, p. 1.

[3] T. W. Crowe, "Opening the Terahertz Window with Integrated Diode Circuits," vol. 40, no. 10, 2005.

[4] T. G. Phillips and J. Keene, "Submillimeter Astronomy," vol. 80, no. 11, 1992.

[5] J. Waters, F. L., W. G. Read, G. L. Manney and L. S. Elson, "Stratospheric C10 and ozone from the microwave limb sounder on the upper atmosphere research satelilite," vol. 362, 1993.

[6] E. R. Mueller, "Terahertz Radiation: Applications and Sources," *The Industrial Physicist*, September 2003.

[7] G. Gallerano and S. Biedron, "Overview of Terahertz Radiation SOurces," in *Proceedings of the 2004 FEL Conference*, Trieste, Italy, 2004.

[8] "Virginia Diodes," 2012. [Online]. Available: http://vadiodes.com/. [Accessed 27 3 2012].

[9] P. F. Bernath, Spectra of Atoms and Molecules, New York: Oxford University Press, 1995.

[10] C. F. Neese, I. R. Medvedev, G. M. Plummer, A. J. Frank, C. D. Ball and F. C. De Lucia, "Compact Submillimeter/Terahertz Gas Sensor With Efficient Gas Collection, Preconcentration, and ppt Sensitivity," vol. 12, no. 8, 2012.

[11] A. B. Fialkov, U. Steiner, S. J. Lehotay and A. Amirav, "Sensitivity and noise in GC-MS: Achieving low limits of detection for diffucult analytes," *International Journal of Mass Spectrometry*, p. 18, 2006.

[12] J. Settlage, W. Gielsdorf and H. Jaeger, "Femtogram level quantitative determination of nitroglycerin and metabolites in human plasma by GC-MS negative ion chemical ionization, single ion monitoring," *Journal of High Resolution Chromatography*, vol. 6, no. 2, pp. 68-71, 1983.

[13] S.-A. Fredriksson, L.-G. Hammarstrom, L. Henriksson and H. Lakso, "Trace determination of alkyl methylphosphonic acids in environmental and biological samples using gas chromatography/negative-ion chemical ionization mass spectrometry and tandem mass spectrometry," *Journal of Mass Spectrometry*, vol. 30, no. 8, pp. 1122-1143, 1995.

[14] C. Townes and S. Geschwind, "Limiting Sensitivity of a Microwave Spectrometer," *Journal of Applied Physics*, vol. 19, no. 8, pp. 795-796, 1948.

[15] F. C. D. Lucia, "The submillimeter: A Spectroscopists View," *Journal pf Molecular Spectroscopy*, vol. 261, pp. 1-17, 2010.

[16] R. Hughes and E. B. Wilson Jr., "A Microwave Spectograph," no. 71, 1947.

[17] H. W. Harrington, J. R. Hearn and R. F. Rauskolb, "The Routine Rotational Microwave Spectrometer," vol. 22, no. 10, 1971.

[18] "QuickSyn Microwave Frequency Synthesizers," 2010. [Online]. Available: http://www.phasematrix.com/pages/Synthesizers.html. [Accessed 27 3 2012].

[19] "Series PCRO," May 2007. [Online]. Available: http://www.herley.com/pdfs/PCRO%20Datasheet.pdf. [Accessed 27 3 2012].

[20] "AD9910," 2010. [Online]. Available: http://www.analog.com/static/imported-files/data_sheets/AD9910.pdf. [Accessed 27 3 2012].

[21] "Scott Method TO-14A/15/17," Scott, 3 2009. [Online]. Available: http://www.alspecialtygases.com/Files/Method_TO_Standards_1516.2.pdf. [Accessed 27 3 2012].

[22] M. Gordon, "GAMESS," Ames Laboratory, [Online]. Available: http://www.msg.ameslab.gov/gamess/gamess.html. [Accessed 18 07 2012].

[23] "The official Gaussian Website," Gaussian Inc., 30 04 2012. [Online]. Available: http://www.gaussian.com/. [Accessed 18 07 2012].

[24] "The Clean Air Act Amendments of 1990 List of Harzardous Air Pollutants," EPA, 1990. [Online]. Available: http://www.epa.gov/ttn/atw/orig189.html. [Accessed 31 May 2012].

[25] "Igor Pro-Overview," 29 4 2007. [Online]. Available: http://www.wavemetrics.com/products/igorpro/igorpro.htm. [Accessed 27 3 2012].

[26] "7100A Volatiles Preconcentrator," 2012. [Online]. Available: http://www.entechinst.com/media/pdfs/catalog/24-25_7100-volatiles-preconcentrator.pdf. [Accessed 27 3 2012].

[27] "10.0 Liter EconoGrab Tedlar Sampling Bag," 2012. [Online]. Available: http://www.zefon.com/store/10.0-liter-econograb-tedlar-sampling-bag.html. [Accessed 27 3 2012].

[28] I. R. Medvedev, F. C. Neese, G. M. Plummer and F. C. De Lucia, "Impact of Atmospheric Clutter on Doppler-limited sensors in the submillimeter/terahertz," vol. 50, no. 18, 2011.

[29] K. Scwartz, A. Pizzini, B. Arendacka, K. Zerlauth, W. Filipiak, A. Schmid, A. Dzien, S. Neuner and M. Lechleitner, "Breath acetone—aspects of normal physiology related to age and gender as determined in a PTR-MS study," *Journal of Breath Research*, vol. 3, p. 9, 2009.

[30] "SilcoNert," 2012. [Online]. Available: http://www.silcotek.com/silcod-technologies/SilcoNert-inert-coating/. [Accessed 27 3 2012].

[31] "Simultaneous Series DT9832 and DT9836 Modules," 2010. [Online]. Available: ftp://ftp.datx.com/Public/Web/Docs/DT9832-DT9836/Simultaneous_Datasheet.pdf. [Accessed 27 3 2012].

[32] N. Karpowicz, H. Zhong, J. Xu, K.-I. Lin, J.-S. Hwang and X.-C. Zhang, "Comparison between pulsed terahertz time-domain imaging and continuous wave terahertz imaging," *Semiconductor Science and Technology*, vol. 20, pp. 293-299, June 2005.

[33] "Molecular Spectroscopy Jet Propulsion Laboratory," California Institute of Technology, 7 June 2012. [Online]. Available: http://spec.jpl.nasa.gov/. [Accessed 11 July 2012].

[34] X. Yin, D. Abbott and B. W-H.Ng, Terahertz Imaging for Biomedical Applications: Pattern Recognition and Tomographic Reconstruction, New York: Springer Sciene+Buisness Media, 2012.

[35] A. Kupiszewski, "The Gyrotron: A High-Frequency Microwave Amplifier," *DSN Progress Report*, pp. 8-12, 1979.